THE JOURNAL OF BIOLOGICAL CHEMISTRY VOL. 291, NO. 25, pp. 13394–13409, June 17, 2016

Transient Receptor Potential Canonical (TRPC)/Orai1-dependent Store-operated Ca^{2+} Channels

*NEW TARGETS OF ALDOSTERONE IN CARDIOMYOCYTES**

Received for publication, September 21, 2015, and in revised form, April 21, 2016 Published, JBC Papers in Press, April 22, 2016, DOI 10.1074/jbc.M115.693911

Jessica Sabourin[‡1], Fiona Bartoli[‡], Fabrice Antigny[§], Ana Maria Gomez[‡], and Jean-Pierre Benitah[‡]

From the [‡]UMR S1180, INSERM, Université Paris-Sud, Université Paris-Saclay, 92296 Châtenay-Malabry, France and [§]UMR S999, INSERM, Université Paris-Sud, Université Paris-Saclay, Centre Chirurgical Marie Lannelongue, 92350 Le Plessis Robinson, France

Store-operated Ca^{2+} entry (SOCE) has emerged as an important mechanism in cardiac pathology. However, the signals that up-regulate SOCE in the heart remain unexplored. Clinical trials have emphasized the beneficial role of mineralocorticoid receptor (MR) signaling blockade in heart failure and associated arrhythmias. Accumulated evidence suggests that the mineralocorticoid hormone aldosterone, through activation of its receptor, MR, might be a key regulator of Ca^{2+} influx in cardiomyocytes. We thus assessed whether and how SOCE involving transient receptor potential canonical (TRPC) and Orai1 channels are regulated by aldosterone/MR in neonatal rat ventricular cardiomyocytes. Molecular screening using qRT-PCR and Western blotting demonstrated that aldosterone treatment for 24 h specifically increased the mRNA and/or protein levels of Orai1, TRPC1, -C4, -C5, and stromal interaction molecule 1 through MR activation. These effects were correlated with a specific enhancement of SOCE activities sensitive to store-operated channel inhibitors (SKF-96365 and BTP2) and to a potent Orai1 blocker (S66) and were prevented by TRPC1, -C4, and Orai1 dominant negative mutants or TRPC5 siRNA. A mechanistic approach showed that up-regulation of serum- and glucocorticoid-regulated kinase 1 mRNA expression by aldosterone is involved in enhanced SOCE. Functionally, 24-h aldosterone-enhanced SOCE is associated with increased diastolic $[Ca^{2+}]_i$, which is blunted by store-operated channel inhibitors. Our study provides the first evidence that aldosterone promotes TRPC1-, -C4-, -C5-, and Orai1-mediated SOCE in cardiomyocytes through an MR and serum- and glucocorticoid-regulated kinase 1 pathway.

The last discovered Ca^{2+} channel family, transient receptor potential canonical (TRPC)[2] and Orai1 channels, is widely expressed, but the role of these channels and the modulation of their expression are not completely understood. Notably, the dysregulation of these important mediators of Ca^{2+}-dependent signal transduction has been involved in a broad range of human diseases such as adenocarcinomas, type 2 diabetes and diabetic nephropathy, human proteinuric kidney disease focal and segmental glomerulosclerosis, severe immunodeficiency, congenital myopathy, chronic pulmonary disease, and ectodermal dysplasia (1, 2). Although predominantly thought of in the context of non-excitable cells, store-operated Ca^{2+} entry (SOCE) by store-operated channels (SOCs) has recently emerged as a potential mechanism to alter Ca^{2+} in the diseased cardiomyocyte. Although still under debate, the prime candidate proteins for SOCs encompass the TRPC channel(s) as non-selective cation channels as well as Orai1, the Ca^{2+} selective pore-forming unit of the Ca^{2+} release-activated Ca^{2+} channel (3). Stromal interaction molecule 1 (STIM1) serves as a Ca^{2+} sensor in the endoplasmic reticulum/sarcoplasmic reticulum (SR), clustering proximal to the plasma membrane to activate Orai1 (4) and TRPC channel(s) (5) when Ca^{2+} stores are depleted. The seven isoforms of the TRPC family (TRPC1–7) have been detected in heart (6) as have Orai1 and STIM1 (7). Functionally, activation of Ca^{2+} influx after the depletion of intracellular Ca^{2+} stores was first identified in embryonic and neonatal murine cardiomyocytes (8, 9) and later in adult ventricular myocytes (10, 11).

However, although it has been shown that SOCE machinery plays a role in modulating SR Ca^{2+} load and cytosolic Ca^{2+} levels in cardiac ventricular myocytes and in HL-1 cells (9, 12, 13), the contribution of SOCE to normal cardiac function is still discussed. Nonetheless, SOCE appears to play an important role in cardiac pathological processes such as hypertrophy and arrhythmia. An increase of TRPC5 and -C6 expression is observed in the failing human heart (14, 15). In several animal models of cardiac hypertrophy and heart failure (HF), up-regulation of TRPC1 (16), -C3 (14), -C6 (17), -C7 (18), Orai1 (19), and STIM1 (20) has been reported. Combining different *in vitro* and *in vivo* approaches, including pharmacological and molecular silencing or overexpression, it has been shown that SOCE, through TRPC1, -C3, -C4, and -C6 channels, Orai1, and STIM1

* This work was supported by *European Section of Aldosterone Council* France, Attractivity Grant 2014 from University of Paris Sud, Agence Nationale de la Recherche Grants ANR-13-BSV1–0023-01 and ANR-15-CE14–0005, and *Cardiovasculaire-Obésité-Rein-Diabète* (CORDDIM) (Région Ile de France). The authors declare that they have no conflicts of interest with the contents of this article.

[1] To whom correspondence should be addressed. Tel.: 33-146-83-52-49; Fax: 33-146-83-54-75; E-mail: jessica.sabourin@u-psud.fr.

[2] The abbreviations used are: TRPC, transient receptor potential canonical; Aldo, aldosterone; caf, caffeine; SR, sarcoplasmic reticulum; HF, heart failure; MR, mineralocorticoid receptor; NRVM, neonatal rat ventricular myocyte; RU, RU-28318; STIM, stromal interaction molecule; SOC, store-operated channel; SOCE, store-operated Ca^{2+} entry; SGK1, serum- and glucocorticoid-inducible kinase 1; YWHAZ, tyrosine 3-monooxygenase/tryptophan 5-monooxygenase activation protein ζ; TBP, TATA box-binding protein; Tg, thapsigargin; qRT-PCR, quantitative RT-PCR; NFAT, nuclear factor of activated T cells; GSK, GSK650394; aa, amino acids; ctrl, control; pF, picofarads; dn, dominant negative; *I-V*, current-to-voltage; I_{SOC}, SOC currents.

are necessary for hypertrophy development and HF by activating calcineurin/NFAT signaling (11, 14–16, 21–26). Furthermore, SOCE potentially has proarrhythmic effects (27–30). SKF-96365, a common inhibitor of SOCs, decreased the number of ventricular tachycardia and early afterdepolarization in mouse hearts expressing constitutively active $G\alpha_q$ with increased TRPC3 and -C6 expression (27). Excessive activation of TRPC3 in a cardiac overexpression mouse model is associated with arrhythmogenesis (31). The Orai activator 2-aminoethoxydiphenyl borate induced an SKF-96365-sensitive automatic activity in rat left ventricular papillary muscles (32). However, although the role of SOCE up-regulation in cardiac pathology is acknowledged, the signaling pathways that govern this up-regulation remain elusive.

Clinical trials have emphasized the high beneficial role of mineralocorticoid receptor (MR) signaling blockade in HF and associated arrhythmias (33). Accumulated evidence suggests that modulation of Ca^{2+} flux is a central factor in the cardiac MR action and might be involved in triggering after depolarization-related fatal ventricular tachyarrhythmia (34–39). In addition, aldosterone-mediated cardiac action may cause various responses associated with elevation of $[Ca^{2+}]_i$, including the direct or indirect increase of the Ca^{2+}-dependent phosphatase 2B calcineurin and its downstream transcription factor NFATc3 in the development of cardiac hypertrophy (40), the negative feedback on cAMP-response element-binding protein via protein phosphatase 2A in promoting apoptosis (41), and more recently the activation of the multifunctional Ca^{2+}/calmodulin-dependent protein kinase II associated with poor outcomes after myocardial infarction (42).

Altogether, these data draw a parallel between the detrimental cardiac effect of aldosterone/MR and SOCE. We thus assessed whether and how SOCE-involved TRPC and Orai1 channels are regulated by cardiac aldosterone/MR signaling in neonatal rat ventricular cardiomyocytes (NRVMs). We showed that aldosterone promotes an MR-specific enhancement of STIM1-dependent SOCE activities, which correlated with the increased expression and activity of TRPC1, -C4, -C5, and Orai1 channels. This effect was dependent on the up-regulation of serum- and glucocorticoid-inducible kinase 1 (SGK1). This is the first demonstration of the cardiac SOCE activation by mineralocorticoid signaling, an effect that might contribute to the benefit of MR blockade in cardiac diseases.

Experimental Procedures

Cell Isolation and Culture—All experiments were carried out according to the ethical principles laid down by the French Ministry of Agriculture and to conform to the guidelines from Directive 2010/63/EU of the European Parliament on the protection of animals. NRVMs were isolated from 1–2-day-old Wistar rats. The heads were cut off, hearts were removed, ventricles were pooled, and ventricular cells were dispersed by successive enzymatic digestion with collagenase A (Roche Applied Science) and pancreatin (Sigma-Aldrich). The cell suspension was purified by centrifugation through a discontinuous Percoll gradient to obtain myocardial cell cultures with 99% myocytes. After seeding on glass coverslips coated with poly-D-lysine (Sigma-Aldrich) in 30-mm plastic wells, NRVMs were cultured in Dulbecco's modified Eagle's medium (DMEM)/Medium 199 (4:1) supplemented with 10% horse serum, 5% fetal bovine serum, 1% glutamine, and antibiotics (plating medium) for 24 h. Approximately 95% of the cells displayed spontaneous contractile activity in culture. Then the cells were cultured in serum-free media for 48 h and treated for 24 h in the presence or absence of various agents.

The mineralocorticoid hormone aldosterone (Aldo), the L-type Ca^{2+} channel inhibitor nifedipine (NIF), the general TRPC channel inhibitor SKF-96365, and the irreversible sarco/endoplasmic reticulum Ca^{2+}-ATPase inhibitor thapsigargin (Tg) were from Sigma-Aldrich. The ryanodine receptor activator caffeine (caf) and the store-operated channel inhibitor BTP2 were purchased from Merck. The Orai1 inhibitor S66 was a kind gift from Richard Foster and David J. Beech (University of Leeds, UK). The Na^+/Ca^{2+} exchanger inhibitor KB-R7943 and the selective antagonist of MR RU-28318 (RU) were purchased from Tocris Bioscience (Bristol, UK). The SGK1 inhibitor GSK650394 (GSK) was from Santa Cruz Biotechnology (Dallas, TX). All compounds were dissolved in DMSO except Aldo and RU, which were diluted in ethanol and water, respectively. All vehicles were diluted at least 1:1000, which had no effect on NRVM function by themselves. Of note, we did not observe cellular hypertrophy measured by planimetry after 24-h 1 μM aldosterone treatment (untreated NRVMs, 788 $\pm$ 21 μm^2, $n = 380$; aldosterone-treated NRVMs, 785 $\pm$ 21 μm^2, $n = 304$).

Cell Transfections—NRVMs were transiently transfected with plasmids or siRNA using Lipofectamine 2000 (Life Technologies) according to the manufacturer's instructions. pMAX-GFP vector was obtained from Amaxa Biosystems (Lonza, Basel, Switzerland). The dominant negative mutants of TRPC1 (F562A) and TRPC4 (E647K/E648K) were a kind gift from Shmuel Muallem (National Institutes of Health, Bethesda, MD) (43), and Orai1-YFP (E106A mutant) construct was from Stephane Koening (University of Geneva, Switzerland). The mutant TRPC3 was a kind gift from Klaus Groschner (University of Graz, Austria) (44). Plasmids YFP-WT-STIM1 (19754) and YFP-STIM1-ΔK (18861) were purchased from Addgene (45). 0.5–2 μg of plasmid or a 200 nM concentration of a specific pool of four different siRNA duplexes (siGENOME SMARTpool siRNA from Life Technologies) against either TRPC5 (M-094467-01-0005) or SGK1 (M-090762-01-0005) or a nontargeting siRNA (D-001210-01-05) used as a negative control and 5 μl of Lipofectamine transfection reagent were mixed in 800 μl of serum-free medium (Opti-MEM). The mixture was incubated for 30 min at 37 °C and added drop by drop in each cell culture dish. After 12–24 h, the Opti-MEM was replaced by the maintenance medium. The cells were kept in culture for a further 48 h until expression of the YFP or GFP fusion protein (as a marker of successful transfection in the case of plasmid transfection) was detectable in the cells. Empty pMAXGFP or pcDNA3-YFP vectors were used as controls to verify whether transfection itself could affect the Ca^{2+} response.

Western Blotting—NRVMs were lysed in a radioimmunoprecipitation assay buffer containing 50 mM Tris-HCl, pH 7.4, 150 mM NaCl, 5 mM EDTA, 1% Triton X-100, 0.05% Nonidet P-40, 0.1% sodium dodecyl sulfate (SDS), and a protease inhibitor

mixture from Roche Applied Science. Samples were denatured in Laemmli buffer for 5 min at 90 °C, and 20–40 μg of total proteins were loaded per lane, separated by 10% SDS-polyacrylamide gel electrophoresis, and transferred to a polyvinylidene difluoride membrane (PVDF; Immobilon®-P, Millipore, Molsheim, France). Membranes were blocked for 1 h with 5% non-fat milk in 1× TBS (20 mM Tris base, 154 mM NaCl, pH 7.4) with 0.2% Tween 20 and probed overnight at 4 °C with primary antibodies (1:200) against rabbit TRPC3 (ACC-016, epitope HKLSEKLNPSVLRC corresponding to amino acids (aa) 822–835), TRPC4 (ACC-018; epitope KEKHAHEEDSSIDYDL corresponding to aa 943–958), TRPC5 (ACC-020; epitope, HKWGDGQEEQVTTRL corresponding to aa 959–973), TRPC6 (ACC-017; epitope, RRNESQDYLLMDELG corresponding to aa 24–38), STIM2 (ACC-064; epitope, SAEKQWEVPDTASEC corresponding to aa 583–597), and Orai3 (ACC-065; epitope, REFVHRGYLDLMGAS corresponding to aa 28–42) from Alomone Labs (Jerusalem, Israel); rabbit Orai1 (O8264; epitope, not provided; peptide corresponding to aa 288–301) and STIM1 (S6197; epitope, not provided; peptide corresponding to aa 657–683) from Sigma-Aldrich; mouse TRPC1 (sc-133076; epitope, not provided; peptide corresponding to aa 689–793), goat SGK1 (sc-15885; epitope, not provided; peptide corresponding to aa 689–793), and mouse β-actin-coupled HRP (1:30,000) from Santa Cruz Biotechnology. After washes, the membranes were incubated in a 1:10,000 dilution of secondary anti-rabbit, anti-mouse, or anti-goat IgG (from Santa Cruz Biotechnology) in TBS containing 2% BSA for 1 h at room temperature. Immunoreactive bands were detected with an enhanced chemiluminescence procedure using the ECL Western Blotting Analysis System (Millipore). The Western blotting quantification was performed with ImageJ software.

Co-immunoprecipitation—After NRVM lysis, 2 μg of antibody was added to a volume of lysate containing 300 μg of proteins diluted with 600 μl of NET solubilization buffer (50 mM Tris-HCl, pH 7.4, 150 mM NaCl, 5 mM EDTA, 0.05% Nonidet P-40 (v/v)) and incubated at 4 °C overnight with constant mixing. Then the incubation continued for 1 h at 4 °C with constant mixing with 50 μl of Protein A/G magnetic beads (Millipore). The immune complexes were collected with a magnetic stand and washed three times in NET solubilization buffer. After denaturing, samples were subjected to SDS-PAGE. The negative control was performed using lysates with beads (ctrl(−)) without any antibody. For technical reasons, it was not possible to perform immunoblotting of Orai1 because its molecular weight is approximately the same as the molecular weight of IgG antibodies.

Immunostaining—NRVMs were fixed and permeabilized in cold 100% methanol for 5 min or with 4% paraformaldehyde and 0.5% Triton X-100 (20 and 5 min, respectively) and washed in 1× TBS containing in 20 mM Tris-HCl, 154 mM NaCl, 2 mM EGTA, 2 mM $MgCl_2$, pH 7.4. A saturation step was executed with TBS plus 1% BSA for 10 min. Samples were incubated for 1 h with primary antibody against STIM1 diluted 1:100 or Orai1, TRPC1, or -C4 diluted 1:25 in TBS plus 1% BSA. After washing in TBS, cells were incubated for 1 h in TBS plus 1% BSA with Alexa Fluor® 594- or 555-conjugated anti-mouse or -rabbit IgG (Life Technologies). The cells were mounted using Mowiol mounting medium. Images were acquired using a Leica TCS SP5 confocal microscope.

Quantitative Real Time PCR Analysis—Total RNA from NRVMs was isolated using the TRIzol procedure (Life Technologies) according to the manufacturer's instructions. For cDNA synthesis, 1 μg of total RNA was reverse transcribed using an iScript cDNA synthesis kit (Bio-Rad) according to the manufacturer's instructions in a total volume of 20 μl. The cDNA was then subjected to five successive dilutions (from 10 to 0.65 ng/μl). Then cDNA was used as a template for real time PCR with SYBR Green Supermix (Bio-Rad) and a 0.5 μM concentration of each primer in a total reaction volume of 15 μl. Cycling conditions were as follows: 30 s at 95 °C followed by 40 cycles of 95 °C for 2 s and 60 °C for 5 s. A dissociation curve was performed with the following steps: 60–95 °C for 5 s with an increment of 0.5 °C. Each sample was tested in duplicate. Quantitative determination of the different mRNA expression levels was performed with a CFX96 Touch™ Real-Time PCR Detection System (Bio-Rad) with either gene-specific primers or primers for YWHAZ, RPL32, and TBP as endogenous controls (Table 1) from Eurofins MWG Operon (France). mRNA levels were normalized to housekeeping genes and were expressed as -fold change of that determined in untreated NRVMs for each culture.

Measurement of Cytosolic Ca^{2+} Changes—NRVMs were rinsed with a physiological solution containing 135 mM NaCl, 5 mM KCl, 1.8 mM $CaCl_2$, 1 mM $MgCl_2$, 10 mM HEPES, 10 mM D-glucose, pH 7.4 with NaOH) and then incubated at 37 °C for 30 min in darkness in the same solution supplemented with 2 μM Fura-2/AM dissolved in DMSO plus 20% Pluronic acid (Life Technologies). Loaded cells were washed twice with the physiological solution before imaging. Ratiometric Fura-2 images of Ca^{2+} signal were obtained using an inverted microscope (Axio Observer.D1, Zeiss) equipped with a Polychrome V fast monochromator system (Till Photonics), which alternately changed the excitation wavelength between 340 and 380 nm. Emission at 510 nm was collected by a cooled, 16-bit electron-multiplying charge-coupled device camera (Evolve, Photometrics) coupled to the microscope (×40 oil immersion fluorescence objective). Image acquisition in selected cells and analysis were performed with Metafluor 7.8 imaging software (Molecular Devices).

To study SOCE in NRVMs, the cells were depleted with 2 μM Tg and 10 mM caffeine in a Ca^{2+}-free solution containing 0.1 mM EGTA in the presence of 10 μM NIF. Subsequently, 1.8 mM Ca^{2+} + NIF were re-added to the medium, and the peak amplitude of the fluorometric signal corresponding to the response to reintroduction of external Ca^{2+} was determined with ΔF (where F is the fluorescence ratio).

The cation influx, was measured as described previously (29). All experiments were done at a controlled 37 °C.

The 340/380 ratios were calibrated using the equation according to Grynkiewicz *et al.* (75): $[Ca^{2+}]_i = K_D \times \beta \times (R - R_{min})/(R_{max} - R)$ where R is the fluorescence ratio recorded at the two excitation wavelengths (F_{340} and F_{380}), K_D represents the dissociation constant, R_{min} and R_{max} are the fluorescence ratios under Ca^{2+}-free and Ca^{2+}-saturating conditions, and $\beta = F_{340}$, zero Ca^{2+} solution/F_{380}, saturating Ca^{2+} solution.

TABLE 1
Primer sequences for PCR amplifications

Primer	Sequence (5′–3′)	Annealing temperature
		°C
TRPC1 forward	TTC CAA AGA GCA GAA GGA CTG	60
TRPC1 reverse	AGG TGC CAA TGA ACG AGT G	
TRPC3 forward	GCA TTC TCA ATC AGC CAA CA	60
TRPC3 reverse	TTC ACC TTC GTT CAC CTC ATC	
TRPC4 forward	AGG CTG GAG GAG AAG ACA CT	60
TRPC4 reverse	CAG GTA GCA CAC GGA GAA GA	
TRPC5 forward	TGA GTG GAA GTT TGC GAG AA	60
TRPC5 reverse	TGG GAC AGA AGG TGT TGT TG	
TRPC6 forward	AGT GTA CAG AAT GCA GCC AGA AAC	60
TRPC6 reverse	CAG CCC TTT GTA GGC ATT GAT C	
STIM1 forward	TCT CTG AGT TGG AGG ATG AGT AGA	60
STIM1 reverse	CAA TAT AGG GGA GCA GAG GTA AGA	
STIM2 forward	GCT AAG GAC GAG GCA GAA AA	60
STIM2 reverse	GGT CCC AAA GAC TGT GCT TC	
ORAI1 forward	ATC GTC TTT GCC GTT CAC TT	60
ORAI1 reverse	AGA GAA TGG TCC CCT CTG TG	
ORAI3 forward	CCA CCA GTC ACC ACA CCA	60
ORAI3 reverse	CCA GCC CAC CAA AAC AAC	
SGK1 forward	CTG CTC GAA GTA CCC TCA CC	60
SGK1 reverse	GCA TGC ATA GGA GTT GTT GG	
RPL32 forward	GCT GCT GAT GTG CAA CAA A	60
RPL32 reverse	GGG ATT GGT GAC TCT GAT GG	
TBP forward	AAA GAC CAT TGC ACT TCG TG	60
TBP reverse	GCT CCT GTG CAC ACC ATT TT	
YWHAZ forward	AGA CGG AAG GTG CTG AGA AA	60
YWHAZ reverse	GAA GCA TTG GGG ATC AAG A	

For *in situ* measurements of R_{min} and R_{max}, Fura-2-loaded cells were first exposed to Ca^{2+}-free solution with 10 mM caffeine + 2 μM thapsigargin for 5 min to empty SR Ca^{2+} stores. Bath solution was then switched to K-buffer (10 mM NaCl, 130 mM KCl, 1 mM $MgCl_2$, 10 mM HEPES, pH 7.2, ionic strength 0.142, 37 °C) containing 10 mM EGTA. To obtain R_{min}, the cells were incubated for 30–45 min with 20 μM non-fluorescent Ca^{2+} ionophore ionomycin (Merck) and 10 μM carbonyl cyanide *p*-trifluoromethoxyphenylhydrazone (Sigma-Aldrich) in K-buffer Ca^{2+}-free solution, and measurements were taken at both wavelengths after the fluorescence reached stable values. Then R_{max} was obtained by saturating the indicator with 10 or 20 mM $CaCl_2$ in the presence of 10 mM EGTA.

To calculate the K_D, a dose response (0, 1.0, 2.0, 3.0, 4.0, 5.0, 6.0, 7.0, 8.0, 9.0, and 10.0 mM $CaCl_2$ and EGTA (free Ca^{2+} ranging from 0 to 37 μM) was performed in K-buffer. As a double log plot, the Ca^{2+} response of the indicator is linear with the x intercept being equal to the log of the apparent K_D of the indicator. We calculated the following values for NRVMs: R_{min} = 0.56, R_{max} = 1.83, and β = 1.55 with K_D = 377 nM. Of note, aldosterone treatment did not change any parameters.

The Fluo-4 signal was recorded with a laser scanning confocal microscope (Leica SP5) equipped with an ×40 water immersion objective. Fluo-4 was excited at 490 nm with a white light laser, and emission was collected at >510 nm. The NRVMs, continuously perfused with physiological saline solution, were paced at 1 Hz. $[Ca^{2+}]_i$ transients were recorded by scanning the cells in XY line mode with a resonant scanner (8000 Hz); the window size used allowed rates of one image/15 ms. The cytosolic Ca^{2+} variation was normalized by dividing the peak fluorescence intensity (F) by the average resting fluorescence intensity (F_0) to generate an F/F_0 image. $[Ca^{2+}]_i$ transient properties as well as the amplitude (maximum F/F_0) or differences in diastolic fluorescence (F_D/F_0), the time to peak (in ms), and the time constant of decay (τ; in ms) were calculated by fitting the decay portion of the fluorescence trace to a monoexponential function. The SOCE measured in NRVMs was recorded by scanning the cells in XY line mode with 700-Hz speed every 387 ms.

Electrophysiological Recordings—The whole-cell patch clamp currents were recorded at room temperature (22 ± 2 °C) using an Axopatch 200B amplifier, filtered at 2 kHz, and digitized at 10 kHz using pClamp 10 software. Borosilicate glass pipettes (Harvard Apparatus) were pulled with a Sutter puller and fire-polished and had a resistance of 3–5 megaohms. The pipette solution contained 135 mM CsCl, 4 mM $MgCl_2$, 5 mM EGTA, 10 mM HEPES, 5 mM Na_2ATP, and 3 mM Na_2 creatine phosphate, pH 7.2 with LiOH, and cells were perfused with a solution containing 132 mM NaCl, 1.1 mM $MgCl_2$, 4 mM CsCl, 10 mM $CaCl_2$, 10 mM glucose, 0.01 mM NIF, 0.05 mM KB-R7943, and 10 mM HEPES, pH 7.4 with LiOH. Series resistance was electronically compensated up to 50% and was continually monitored during the experiment. Membrane capacitances (9–15 pF) were measured for each cell with pClamp 10 software. The SR Ca^{2+} stores were depleted by 2 μM Tg and 10 mM caf, and the SOC currents (I_{SOC}) were elicited by a 1.2-s voltage ramp from −100 to + 60 mV preceded by a 0- to +40-mV prepulse (400 ms) to inactivate the voltage-dependent Na^+ channels.

The currents were recorded before and after 5 μM BTP2 cell perfusion and then normalized to membrane capacitance to account for cell size variations. The slope conductance was calculated according to the formula: $\Delta I/\Delta V_m = I_{-90\,mV} - I_{+60\,mV})/(-90 - 60\,mV)$.

Statistical Analysis—All analysis was performed with GraphPad Prism 6 software. All values are reported as mean ± S.E. For all experiments, the difference between two groups was assessed with two-tailed unpaired Student's *t* test and among at

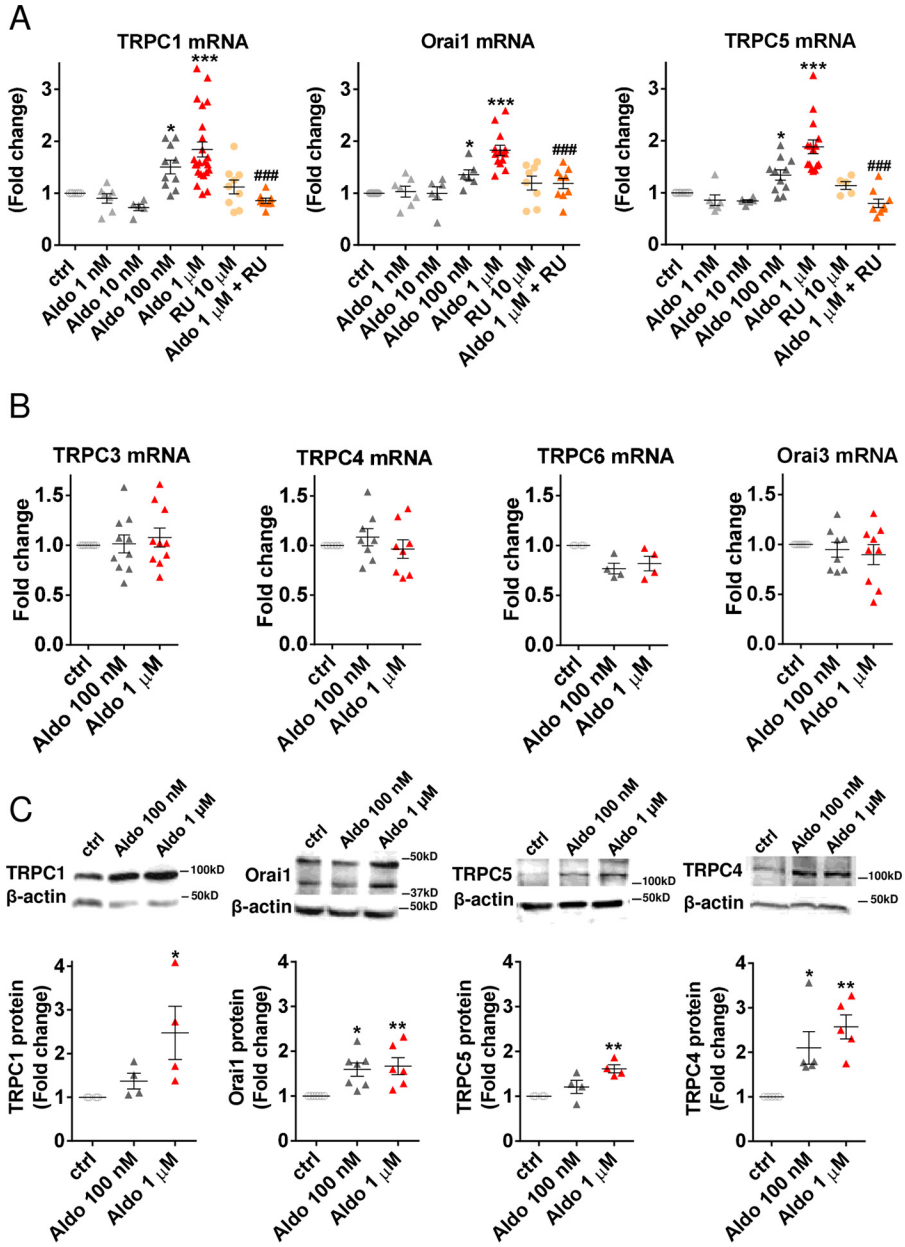

FIGURE 1. **24-h aldosterone treatment increases mRNA and protein expression of SOCs.** *A*, TRPC1, Orai1, and TRPC5 mRNA expression (*panels* from *left* to *right*) relative to control was determined by qRT-PCR. NRVMs were incubated for 24 h in the absence or presence of 1 nM, 10 nM, 100 nM, or 1 μM Aldo alone or in combination with 10 μM selective MR antagonist RU. mRNA levels were normalized to housekeeping genes and expressed as -fold change of that determined in untreated NRVMs for each culture. *Error bars* represent S.E. *, $p < 0.05$; ***, $p < 0.001$ *versus* ctrl; ###, $p < 0.001$ *versus* Aldo; $n = 5$–23 primary cultures. *B*, relative TRPC3, -C4, -C6, and Orai3 mRNA expression (from *left* to *right*) in NRVMs incubated for 24 h in the absence (ctrl) or presence of 100 nM or 1 μM Aldo. $n = 4$–10 primary cultures. *C*, TRPC1, Orai1, TRPC5, and -C4 protein expression (*panels* from *left* to *right*) relative to control was determined by Western blotting. Protein levels were normalized by β-actin and expressed as -fold change of that determined in untreated NRVMs for each culture. *Error bars* represent S.E. *, $p < 0.05$; **, $p < 0.01$ *versus* ctrl; $n = 4$–7 primary cultures.

least three groups was assessed with one-way or two-way analysis of variance completed by Fisher's least significant difference post hoc test for multiple comparisons. The statistical significance was defined by a value of $p \leq 0.05$.

Results

Aldosterone Increases TRPC1, -C4, -C5, and Orai1 Expression—We first investigated the effect of 24-h aldosterone treatment on TRPC and Orai channel expression on NRVMs. The mRNA expression of TRPC1, -C3–C6, Orai1, and Orai3 in aldosterone-treated NRVMs was compared with untreated NRVMs using qRT-PCR. TRPC2 and -C7 isoforms were undetectable by classical PCR in our cells. As shown in Fig. 1*A* (from *left* to *right panels*), the mRNA levels of TRPC1, Orai1, and TRPC5 were significantly increased by 100 nM and 1 μM aldosterone treatment, whereas lower doses (1 and 10 nM) had no effect. The effects were totally prevented when NRVMs were co-incubated for 24 h with the selective MR antagonist (10 μM RU; Fig. 1*A*). By contrast, the mRNA levels of TRPC3, -C4, -C6, and Orai3 were unchanged after aldosterone treatment (Fig. 1*B*). These results were correlated to the increased expression of TRPC1, Orai1, and TRPC5 protein levels (Fig. 1*C*). Of inter-

est, we observed an increased expression of TRPC4 at the protein level (Fig. 1*C*, *right panel*) in aldosterone-treated cells, whereas TRPC3, -C6, and Orai3 proteins were not affected (data not shown).

Aldosterone Increases SOCE Sensitive to BTP2 and SKF-96365 via MR Activation—Because TRPC1, -C4, -C5, and Orai1 form functional SOCs in a variety of cell types, we then investigated the effect of 24-h aldosterone treatment on SOCE in NRVMs. Variation of $[Ca^{2+}]_i$ following the depletion of intracellular Ca^{2+} stores was measured on Fluo-4-loaded NRVMs. As shown in Fig. 2*A*, *left panel*, store depletion in Ca^{2+}-free solution with 2 μM Tg and 10 mM caf in the presence of 10 μM NIF induced a large Ca^{2+} release from the SR in NRVMs. The amplitude of the Ca^{2+} release was not modified after aldosterone treatment, suggesting that the SR Ca^{2+} load is unaltered as observed in adult cardiomyocytes (39). When Ca^{2+} was reintroduced (in the presence of NIF), a moderate SOCE was recorded in untreated NRVMs (ctrl, *light gray* trace), whereas a large SOCE was observed in the aldosterone-treated NRVMs (100 nM, *dark gray* trace; 1 μM, *red* trace). On average, chronic treatment with 100 nM and 1 μM aldosterone significantly increased SOCE by up to 1.8-fold (Fig. 2*A*, *right panel*). These effects were prevented with 24-h exposure to the MR antagonist RU (Fig. 2*A*). In addition, a lower aldosterone concentration (10 nM; Fig. 2*A*) or acute 1 μM aldosterone exposure for 5 min (data not shown) did not affect SOCE in NRVMs. A pharmacological strategy using 5 μM BTP2 or 40 μM SKF-96365, widely used SOC inhibitors, decreased SOCE in control cells but also strongly prevented the enhanced SOCE induced by aldosterone treatment (Fig. 2*B*). Of note, 5 μM KB-R7943, a Na^+/Ca^{2+} exchanger blocker, did not alter SOCE in NRVMs treated or not with aldosterone (data not shown). To obtain direct evidence that exacerbated SOCE induced by aldosterone is closely linked to SOC activity, we measured the Mn^{2+}-induced quenching of Fura-2 fluorescence as an indicator of Ca^{2+} influx. Fig. 2*C*, *left panel*, shows representative traces of the progressive decay phase of Fura-2 fluorescence after 500 μM Mn^{2+} addition to NRVMs cultured in the presence (*red* trace) or absence (*light gray* trace) of 1 μM aldosterone. On average, we observed a 2.4-fold increased cation entry through SOCs with aldosterone treatment (Fig. 2*C*, *right panel*).

Aldosterone Enhanced SOCE Is Dependent on TRPC1, -C4, -C5, and Orai1 Channels—To confirm the molecular candidates for aldosterone-enhanced SOCE, NRVMs were transiently transfected either with the dominant negative construct for TRPC1 (F562A; dn-TRPC1), TRPC4 (E647K/E648K; dn-TRPC4), TRPC3 (N-terminal fragment (aa 1–302); dn-TRPC3), or YFP-Orai1 (E106A; dn-Orai1) 24 h before treatment (43, 44, 46, 47). The successful expression at the plasma membrane of the dominant negative (dn) constructs was illustrated by immunostaining of Orai1-YFP and co-immunostaining of TRPC1 or -C4 with GFP tag (Fig. 3*A*, *top panel*). The untreated NRVMs overexpressing either dn-Orai1, dn-TRPC1, or dn-TRPC4 exhibited significantly less SOCE compared with empty pMAX-GFP-transfected cells, and this procedure prevented the aldosterone-increased SOCE (Fig. 3*A*). The remaining SOCE was similar to that in untreated cells. As a negative control, we observed that dn-TRPC3 did not alter SOCE responses

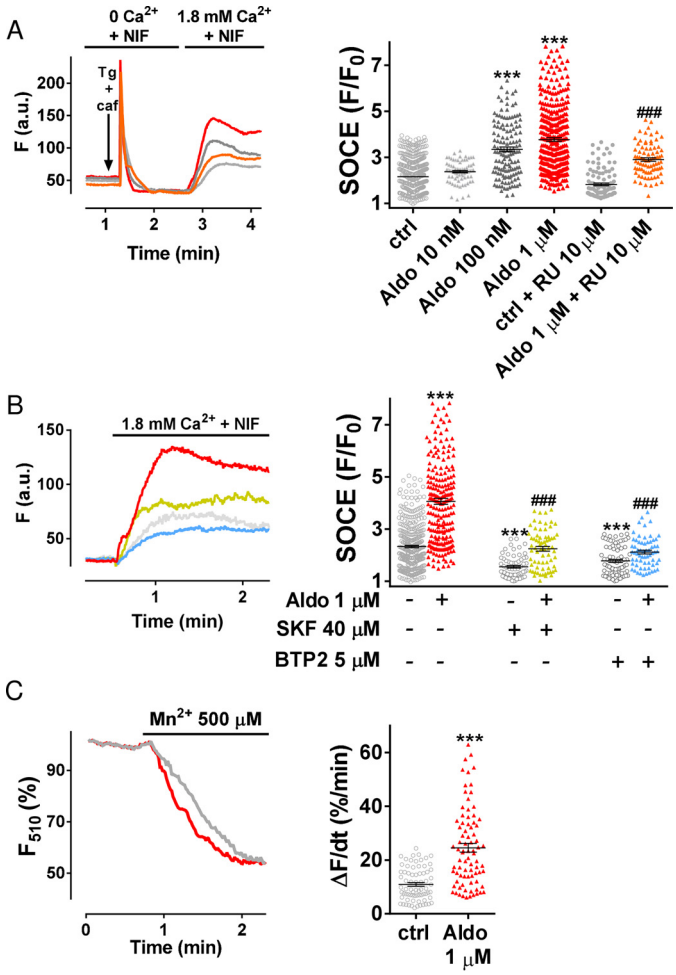

FIGURE 2. **24-h aldosterone treatment increases SOCE.** *A*, *left panel*, representative traces of fluorescence variation in Fluo-4/AM-loaded NRVMs incubated in the absence (*light gray* trace), in the presence of Aldo (100 nM, *dark gray* trace; 1 μM, *red* trace), or in presence of 1 μM Aldo + 10 μM RU (the selective MR antagonist; *orange* trace). Cells were exposed to 2 μM Tg + 10 mM caf in the presence of 10 μM NIF in Ca^{2+}-free medium and then to Ca^{2+}-containing solution to evaluate the SOCE. *Right panel*, scatter plots with mean ± S.E. illustrating amplitude of SOCE (F/F_0) in NRVMs incubated for 24 h in the absence (ctrl; *open circles*) or presence of Aldo (*triangles*; 10 nM, *light gray*; 100 nM, *dark gray*; 1 μM, *red*) without or with a 10 μM concentration of the selective MR antagonist RU (*gray circles* and *orange triangles*). *Error bars* represent S.E. ***, $p < 0.001$ *versus* ctrl; ###, $p < 0.001$ *versus* Aldo; $n = 3$–15 primary cultures; $n = 79$–250 investigated cells. *B*, *left panel*, representative traces of SOCE in Fluo-4/AM-loaded NRVMs incubated in the absence (*light gray* trace), presence of 1 μM Aldo (*red* trace), presence of 1 μM Aldo + 40 μM SKF-96365 (*SKF*; *yellow* trace), or presence of 1 μM Aldo + 5 μM BTP2 (*light blue* trace). *Right panel*, quantitative assessment of SOCE in the ctrl (*open circles*) or Aldo condition (*triangles*) in the absence or presence of SOC inhibitor (5 μM BTP2 or 40 μM SKF-96365). *Error bars* represent S.E. ***, $p < 0.001$ *versus* ctrl; ###, $p < 0.001$ *versus* Aldo; $n = 3$–15 primary cultures; $n = 64$–250 investigated cells. *C*, *left panel*, representative fluorescence traces of the Fura-2 decay phase upon Mn^{2+} addition in untreated (*gray* trace) or 1 μM Aldo-treated (*red* trace) NRVMs. *Right panel*, the initial slope of the Mn^{2+}-induced decrease of Fura-2 fluorescence was fitted by linear regression. Scatter plots with mean ± S.E. illustrate ($\Delta F/dt$) for NRVMs incubated for 24 h with or without 1 μM Aldo. *Error bars* represent S.E. ***, $p < 0.001$ *versus* ctrl; $n = 3$ primary cultures; $n = 76$–95 investigated NRVMs. *a.u.*, arbitrary units.

in NRVMs treated or not with aldosterone (Fig. 3*A*, *bottom panel*). In addition, specific blockade of Orai1 channel with S66 at 1 μM (48) significantly reduced SOCE in untreated and aldosterone-treated NRVMs, validating the dominant negative strategy for Orai1 (Fig. 3*B*). Note that blocking one of these molecular candidates is sufficient to blunt the aldosterone-in-

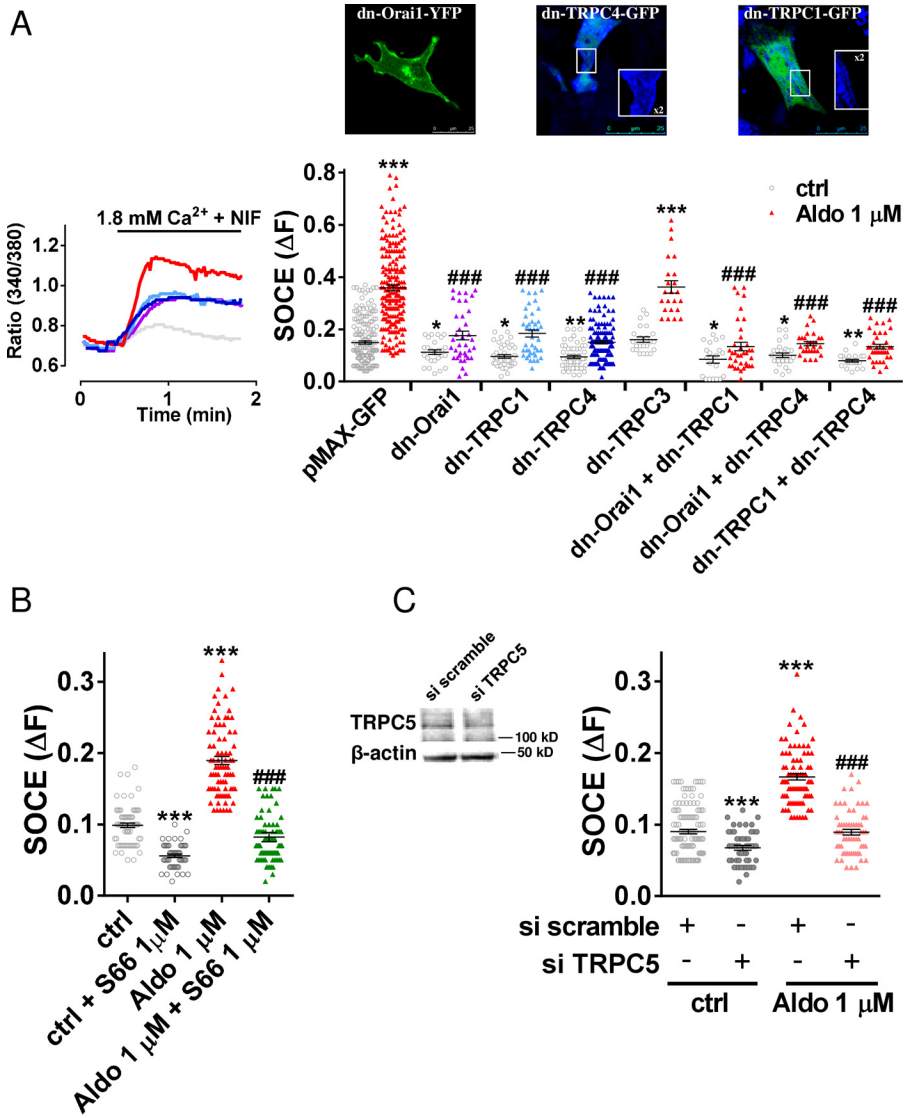

FIGURE 3. **24-h aldosterone treatment increases SOCE via TRPC1, -C4, -C5, and Orai1 channels.** *A*, *left panel*, representative traces of $[Ca^{2+}]_i$ variation measured with Fura-2 fluorescence ratio (340/380) in untreated (pMAX-GFP; *light gray* trace) and Aldo-treated NRVMs previously transfected with pMAX-GFP (*red* trace), YFP-Orai1-E106A (*purple* trace; dn-Orai1), TRPC4-E647K/E648K (*dark blue* trace; dn-TRPC4); or TRPC1-F562A mutant (*blue* trace; dn-TRPC1). *Right panel*, quantitative assessment of SOCE (Δ*F*) from transfected cells. *Error bars* represent S.E. *, $p < 0.05$; **, $p < 0.01$; ***, $p < 0.001$ *versus* ctrl transfected cells; ###, $p < 0.001$ *versus* Aldo transfected cells; $n = 4$ primary cultures; $n = 28–209$ investigated cells. *Top panel*, representative confocal imaging (from *left* to *right*) of YFP-Orai1, GFP-TRPC4, and -C1 signals from transfected NRVMs. *B*, quantitative assessment of SOCE (Δ*F*) in the ctrl or Aldo condition in the absence or presence of Orai1 channel inhibitor S66 (1 μM). *Error bars* represent S.E. ***, $p < 0.001$ *versus* ctrl; ###, $p < 0.001$ *versus* Aldo; $n = 3$ primary cultures; $n = 50–90$ investigated cells. *C*, *left panel*, illustrates a reduction by 35% of the amount of TRPC5 protein after siRNA treatment. *Right panel*, quantitative assessment of SOCE from transfected NRVMs with non-targeted siRNA (*si scramble*) or with a specific siRNA pool against TRPC5 treated with or without Aldo for 24 h. *Error bars* represent S.E. ***, $p < 0.05$ *versus* ctrl transfected cells; ###, $p < 0.001$ *versus* Aldo-transfected cells; $n = 3$ primary cultures; $n = 50–120$ investigated cells.

creased SOCE. In addition, the co-expression of dn-Orai1 and dn-TRPC1, dn-Orai1 and dn-TRPC4, or dn-TRPC1 and dn-TRPC4 mutants did not have an additional effect on SOCE reduction (Fig. 3*A*).

This dominant negative strategy has the advantage to functionally block the target channel without affecting its endogenous expression, which might induce compensatory regulation of other channels. In a first attempt, we also tried dn-TRPC5 (49); however, in our hands, this construct was not expressed in NRVMs and thus we used an siRNA strategy. The knocked down expression of TRPC5 by a specific siRNA pool (four different siRNA duplexes against TRPC5), which reduced the TRPC5 mRNA level by 50% (data not shown) and protein level by 35% (Fig. 3*C*, *left panel*), significantly reduced SOCE in untreated and aldosterone-treated cells compared with scrambled siRNA-transfected NRVMs (Fig. 3*C*, *right panel*). These results suggested that TRPC1, -C4, and -C5 together with Orai1 form functional heterotetramer SOCs as proposed in other cell types (50–52).

Aldosterone Increases I_{SOC} Involving an Assembly of TRPC1, -C4, -C5, and Orai1—To further explore the nature of TRPC/Orai1-dependent SOCs in untreated and aldosterone-treated NRVMs, we measured the store-dependent current using patch clamp in a whole-cell configuration under conditions in which major protagonists controlling the increase in intracellular Ca^{2+} concentration (L-type Ca^{2+} channel, Na^+/Ca^{2+} exchanger, and sarco/endoplasmic reticulum Ca^{2+}-ATPase pump) were blocked. Following SR Ca^{2+} depletion (induced by

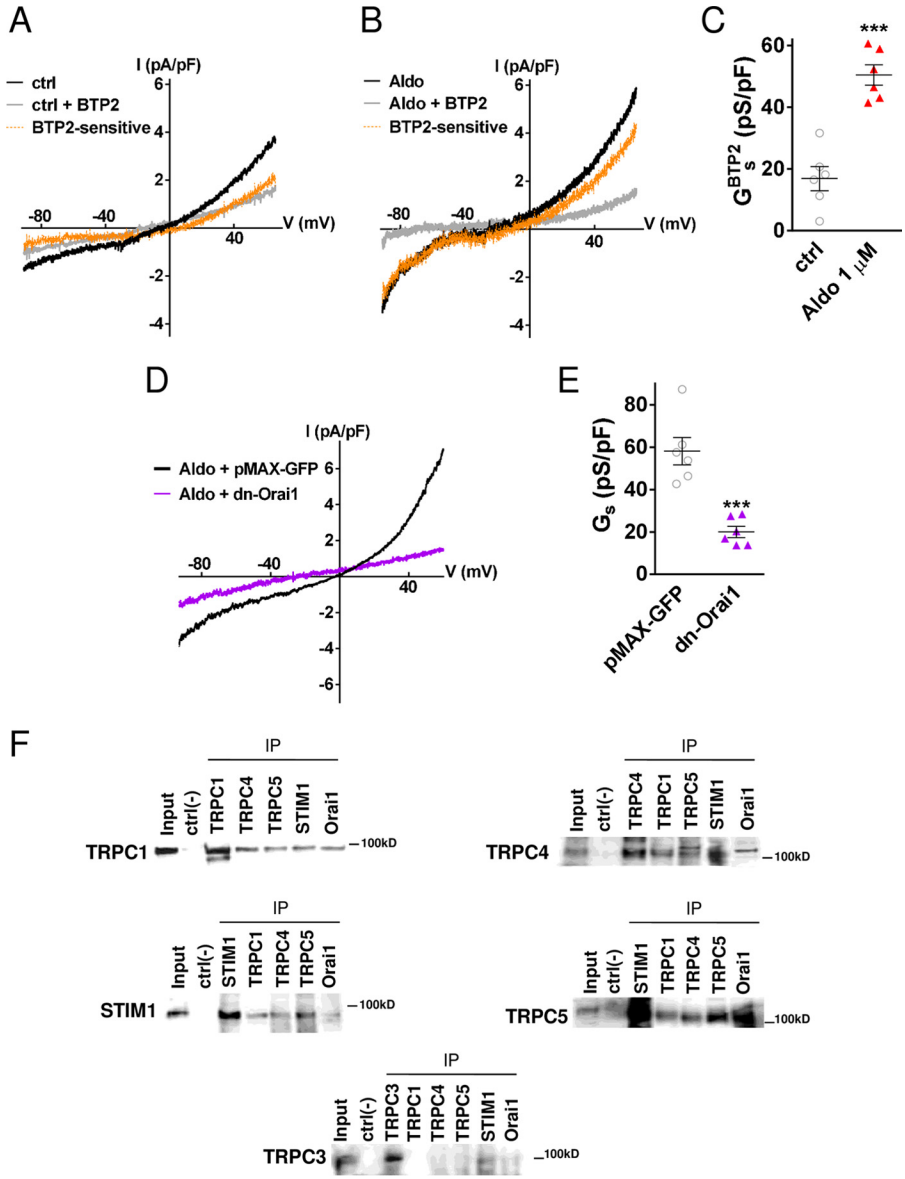

FIGURE 4. **24-h aldosterone treatment increases I_{SOC}.** *A* and *B*, representative *I-V* relationships elicited by a ramp voltage clamp protocol in NRVMs incubated without (ctrl; *A*) or with 1 μM Aldo for 24 h (*B*) following SR Ca^{2+} depletion by 2 μM Tg and 10 mM caf in the absence (*black* traces) or presence of 5 μM BTP2 (*gray* traces). The BTP2-sensitive current (*orange* traces) is the difference current. All solutions contained 10 μM nifedipine and 5 μM KB-R7943. *C*, scatter plots with mean ± S.E. illustrating the BTP2-sensitive I_{SOC} slope conductance (G_s) in picosiemens (*pS*)/pF of NRVMs incubated for 24 h without (ctrl) or with 1 μM Aldo. *Error bars* represent S.E. ***, $p < 0.001$ *versus* ctrl; $n = 6$ investigated cells. *D*, representative *I-V* relationships in Aldo-treated cells expressing the empty pMAX-GFP (*black* trace) or dn-Orai1 mutant plasmid (*purple* trace). *E*, scatter plots with mean ± S.E. illustrating I_{SOC} slope conductance. $n = 6$ investigated cells. *F*, representative co-immunoprecipitation experiments in NRVMs. TRPC1, -C4, -C5, and Orai1 channels and STIM1 formed a macromolecular complex. Lysates (*Input lane*) from NRVMs treated or not with 2 μM Tg + 10 mM caf for 10 min were incubated with antibodies against TRPC1, -C3, -C4, -C5, -STIM1, or Orai1 (*IP*). Western blots of the immunoprecipitated proteins were probed with antibodies against STIM1, TRPC1, -C4, -C5, and -C3 in the depleted condition.

2 μM Tg and 10 mM caf in the presence of 10 μM NIF and 5 μM KB), a standard ramp protocol elicited an almost linear current-to-voltage (*I-V*) relationship in untreated NRVMs (Fig. 4*A*). On average (10 cells), the Tg/caf-induced current densities were −2.4 ± 0.5 and 3.3 ± 0.4 pA/pF at −80 and +60 mV, respectively. Perfusion with 5 μM BTP2 slightly reduced both inward and outward currents. As a result, the BTP2-sensitive current was very low in control cells (on average −0.9 ± 0.4 and 1.3 ± 0.3 pA/pF at −80 and +60 mV, respectively). In cells incubated in the presence of 1 μM aldosterone for 24 h (Fig. 4*B*), we observed robust increases in both inward and outward currents (on average (nine cells) −4.2 ± 0.6 and 5.9 ± 0.8 pA/pF at −80 and + 60 mV, respectively; $p < 0.05$ *versus* ctrl) compared with untreated NRVMs. The aldosterone-enhanced I_{SOC} was virtually abolished in the presence of BTP2, resulting in a much steeper BTP2-sensitive current than that found in untreated NRVMs (−3.0 ± 0.5 and 3.5 ± 0.2 pA/pF at −80 mV and +60 mV, respectively; $p < 0.05$ *versus* ctrl). The slope conductance of the BTP2-sensitive current was significantly enhanced in the aldosterone condition (Fig. 4*C*). The nature of these aldosterone-enhanced I_{SOC} induced by SR depletion that was reversed around 0 mV and presented slight rectification properties suggested the activation of non-selective cationic channels sensitive to SOC blocker. As shown in Fig. 4, *D* and *E*, we observed

that the I_{SOC} (dn-Orai1, -1.07 ± 0.35 and 2.6 ± 0.5 pA/pF at -80 mV and $+60$ mV, respectively; GFP, -3.82 ± 0.66 and 6.1 ± 1.2 pA/pF at -80 mV and $+60$ mV, respectively; $p < 0.05$ *versus* GFP) and the slope conductance were significantly reduced in aldosterone-treated NRVMs expressing dn-Orai1 in comparison with those expressing control plasmid. These results suggested a mixed nature of I_{SOC} carried by TRPC and Orai1 channels.

To further investigate whether TRPC1-, -C4-, and -C5-Orai1-STIM1 could function as channel complexes driving SOCE, we performed co-immunoprecipitation experiments. In depleted NRVMs (induced by Tg and caf for 10 min), TRPC1, -C4, -C5, Orai1, and STIM1 all interacted together (Fig. 4*F*), suggesting that all these proteins might form a macromolecular complex and constitute one functional channel. Of note, TRPC3 only interacts with STIM1. These results are consistent with the idea that SOC function requires Orai1 and that TRPC and Orai1 might contribute to the same channel.

Aldosterone Regulates the SR Ca^{2+}-sensing Protein STIM1—Multiple studies have shown that STIM1 and to a lesser extent STIM2 are central regulators of SOCE. We thus investigated whether aldosterone regulate STIM expression and activity in NRVMs. As shown in Fig. 5*A*, the mRNA levels of STIM1 and STIM2 were unchanged after 24-h aldosterone treatment. However, increased protein expression was observed for STIM1 after aldosterone treatment, whereas the STIM2 protein level was unaffected (Fig. 5*B*). Moreover, immunocytochemical staining showed higher labeling of endogenous STIM1 in aldosterone-treated NRVMs compared with untreated NRVMs (ctrl) with the STIM1 pattern becoming more punctum-like (Fig. 5*C*, *top panels*). Images from NRVMs transfected with YFP-WT-STIM1 also illustrated the punctum pattern of STIM1 in the aldosterone condition (Fig. 5*C*, *bottom panels*). To assess the requirement for STIM1 signaling in the aldosterone-enhanced SOCE, NRVMs were transiently transfected, 24 h before treatment, either with YFP-WT-STIM1 or with the dominant negative construct for STIM1 deleted in its Lys-rich domain (YFP-STIM1-ΔK) (53), preventing an appropriate anchoring of STIM1 in the plasma membrane and activation of TRPC channel(s) but not Orai1 channels. In untreated cells (ctrl) expressing WT-STIM1, SOCE was drastically increased compared with empty pMAX-GFP-transfected cells. Interestingly, in aldosterone-treated cells, WT-STIM1 overexpression had no additional effect on SOCE, suggesting that the STIM1-dependent SOCE machinery is already entirely activated by aldosterone treatment (Fig. 5*D*). In addition, in cells expressing STIM1-ΔK, the aldosterone increase in SOCE was slightly smaller. Aldosterone-enhanced I_{SOC} in STIM1-ΔK-expressing cells confirmed the slight/absent role of the Lys-rich domain of STIM1 in activation of I_{SOC} (Fig. 5, *E* and *F*).

SGK1 Regulates Orai1 Expression and SOCE—Because aldosterone-induced up-regulation of SOCs was observed only for a high dose (Figs. 1 and 2), we suspected the involvement of an intermediate factor. Among the classical aldosterone-induced proteins, SGK1, which is expressed in the heart, constitutes a novel and powerful modulator of SOCE, in particular of Orai1 (54). We thus investigated whether SGK1 might be involved in aldosterone-enhanced SOCE in NRVMs. Compared with untreated NRVMs, aldosterone-treated NRVMs showed a dose-dependent increased SGK1 expression at the mRNA level from low doses of aldosterone (Fig. 6*A*). Co-incubation for 24 h with the SGK1 inhibitor (1 μM GSK) slightly decreased SOCE in control cells and strongly reduced the aldosterone-increased SOCE (Fig. 6*B*). In addition, NRVMs transfected with specific SGK1 siRNA, which reduced the SGK1 mRNA level by 50% (data not shown) and protein level by 51% (Fig. 6*B*, *top panel*), reduced SOCE in aldosterone-treated cells compared with scrambled siRNA-transfected or non-transfected NRVMs (Fig. 6*B*, *bottom panel*). GSK co-incubation with aldosterone did not affect the increased mRNA expression of TRPC1 and -C5 but prevented the increase of Orai1 mRNA levels (Fig. 6*C*), suggesting that SGK1 might constitute a key regulator of the cardiac SOC-mediated Ca^{2+} signaling dependent, at least, on Orai1.

Aldosterone Induces Diastolic Ca^{2+} Increase during Stimulation Involving SOCs—We further investigated the effect of 24-h 1 μM aldosterone treatment on $[Ca^{2+}]_i$ transients. Fig. 7*A*, *top panel*, displays examples of the confocal images obtained in NRVMs electrically stimulated at 1 Hz and incubated for 24 h in the absence (*a*, *b*, and *c*) or presence (*a*′, *b*′, and *c*′) of aldosterone. Compared with untreated NRVMs (Fig. 7*A*, *bottom*, *left panel*), where each stimulus induced a transient rise of $[Ca^{2+}]_i$ (*b*) returning to baseline during diastole (*a* and *c*), aldosterone treatment led to $[Ca^{2+}]_i$ transients that failed to completely relax (Fig. 7*A*, *a*′, *b*′, and *c*′, *bottom*, *right panel*). This behavior was consistently observed for all aldosterone-treated NRVMs and eventually induced a brief period of excitability loss (data not shown). Analysis of the fluorescence signal revealed a striking increase in the diastolic $[Ca^{2+}]_i$, maintained over time during stimulation (data not shown), expressed as the ratio F_D/F_0 (where F_D is fluorescence level at the diastolic period during 1-Hz stimulation and F_0 is the basal fluorescence before stimulation) with aldosterone treatment (Fig. 7*B*). We also observed that the resting $[Ca^{2+}]_i$, measured by the ratiometric Ca^{2+} indicator Fura-2, was significantly increased in aldosterone-treated cells (141.8 ± 0.8 nM, $n = 674$ *versus* 98.4 ± 0.4 nM in control cells, $n = 793$; $p < 0.001$). Interestingly, we observed that this aldosterone-increased resting $[Ca^{2+}]_i$ was reduced in cells transfected with dn-Orai1 (98.4 ± 1.6 nM, $n = 74$; $p < 0.001$ *versus* Aldo), dn-TRPC1 (106 ± 1.5 nM, $n = 73$; $p < 0.001$ *versus* Aldo), or dn-TRPC4 (107.4 ± 2.6 nM, $n = 45$; $p < 0.001$ *versus* Aldo) and with siRNA against TRPC5 (103 ± 1.6 nM, $n = 120$; $p < 0.001$ *versus* Aldo). Consistently, exposure of aldosterone-treated NRVMs to either SOC inhibitor (3 μM BTP2) (Fig. 7*C*) or Orai1 blocker (1 μM S66) for 2–3 min (Fig. 7*D*) significantly reduced the diastolic $[Ca^{2+}]_i$ increase during stimulation. In addition, the co-incubation of aldosterone with GSK for 24 h significantly reduced the diastolic $[Ca^{2+}]_i$ increase (Fig. 7*E*), showing that SGK1 might be a regulator of the cardiac SOC-mediated Ca^{2+} signaling.

Discussion

Accumulated evidence has shown that aldosterone/MR signaling plays a pivotal role in impairing cardiac Ca^{2+} handling as a trigger of ventricular arrhythmias and sudden cardiac death in HF. However, to date, the cellular mechanism of action remains to be more precisely defined. In this context, it is imperative to

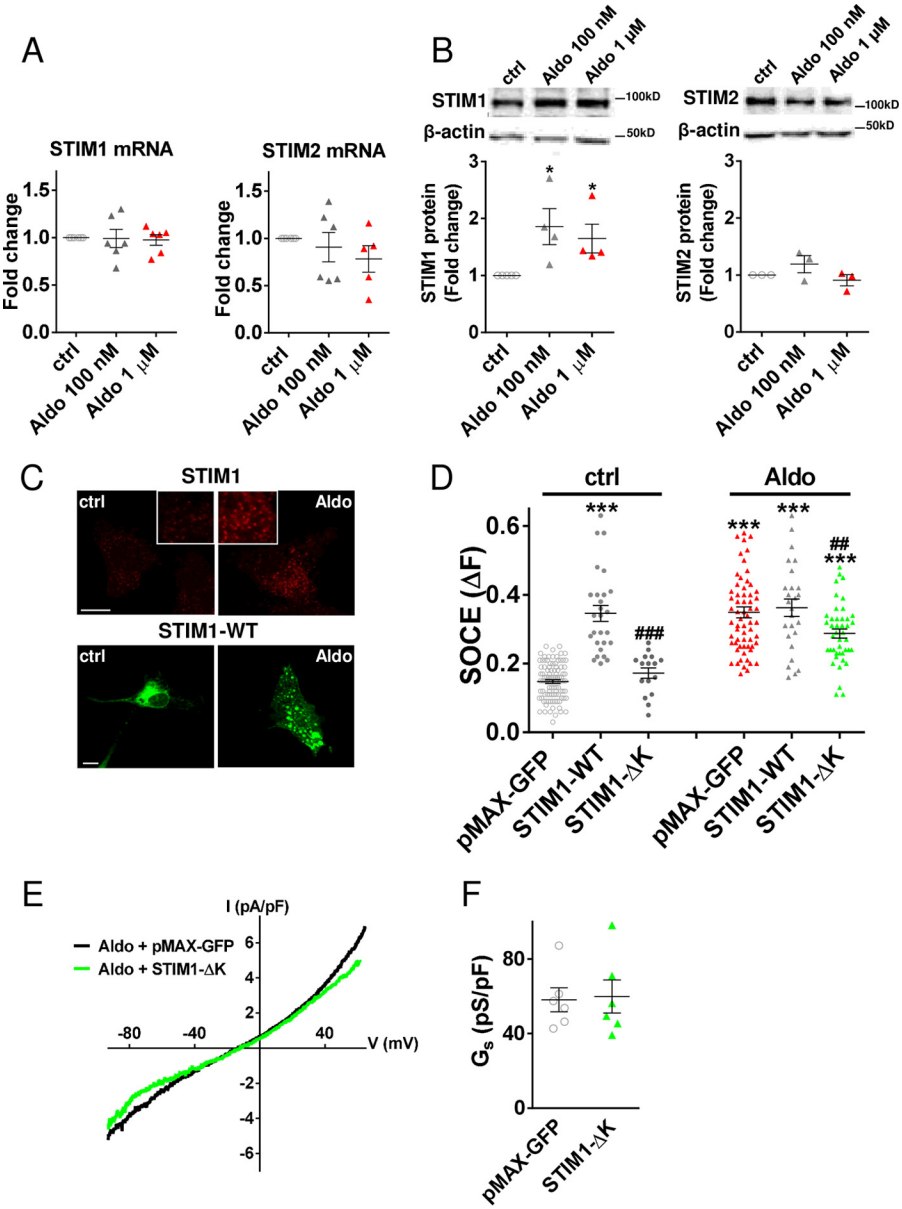

FIGURE 5. **24-h aldosterone treatment increases SOCE partially via STIM1 protein.** *A*, relative STIM1 and STIM2 mRNA expression in NRVMs incubated for 24 h in the absence (ctrl) or presence of 100 nM or 1 μM Aldo. mRNA levels were normalized to housekeeping genes and expressed as -fold change of that determined in untreated NRVMs for each culture. $n = 5–6$ primary cultures. *B*, STIM1 and STIM2 protein expression relative to control was determined by Western blotting. Protein levels were normalized by β-actin and expressed as -fold change of that determined in untreated NRVMs for each culture. *Error bars* represent S.E. *, $p < 0.05$ *versus* ctrl; $n = 3–4$ primary cultures. *C*, immunofluorescence for endogenous STIM1 (*top panel*) and exogenous YFP-WT-STIM1 (*bottom panel*) on NRVMs treated or not (ctrl) with 1 μM Aldo for 24 h. *Scale bars*, 10 μm. *D*, quantitative assessment of SOCE (ΔF) from cells transfected with pMAX-GFP, native YFP-WT-STIM1 (*STIM1-WT*), or YFP-STIM1-ΔK (*STIM1-ΔK*) in ctrl (*circles*) and Aldo (*triangles*) conditions. *Error bars* represent S.E. ***, $p < 0.001$ *versus* ctrl transfected cells; ##, $p < 0.01$; ###, $p < 0.001$ *versus* Aldo-treated WT-STIM1-transfected cells; $n = 3$ primary cultures; $n = 16–63$ investigated cells. *E*, representative *I-V* relationships in Aldo-treated cells expressing the empty pMAX-GFP (*black* trace) or STIM1-ΔK plasmid (*green* trace). *F*, scatter plots with mean ± S.E. illustrating I_{SOC} slope conductance. $n = 6$ investigated cells. *pS*, picosiemens.

identify and characterize new cardiac MR-specific downstream targets. Our study provides the first quantitative description of aldosterone/MR effects upon the SOCs in the heart. After 24-h treatment of NRVMs with aldosterone, we observed an MR-specific enhancement of SOCE, which is correlated to the increased expression and activity of the Ca^{2+} sensor STIM1 and TRPC1, -C4, -C5, and Orai1 channels. Further mechanistic data showed that aldosterone/MR activation of Orai1-dependent SOCE involves SGK1 up-regulation.

Different reports have demonstrated the expression and activity of SOCs in the heart. SOCE appears to be developmentally dependent with greater amplitude in embryonic and neonatal cardiomyocytes but variable and limited in adult cardiomyocytes (7). Consistent with these studies, using a combination of functional Ca^{2+} imaging, electrophysiological, and biochemical approaches, we showed that SOCE is active in NRVMs and is associated with the co-existence of all TRPC isoforms (except TRPC2 and -C7), STIM1/2, and Orai1/3.

We found that chronic aldosterone treatment significantly increased store depletion-induced Ca^{2+} influx in cardiomyocytes. This is consistent with the finding of aldosterone-dependent up-regulation of SOCE in two other cell types (A7r5 rat

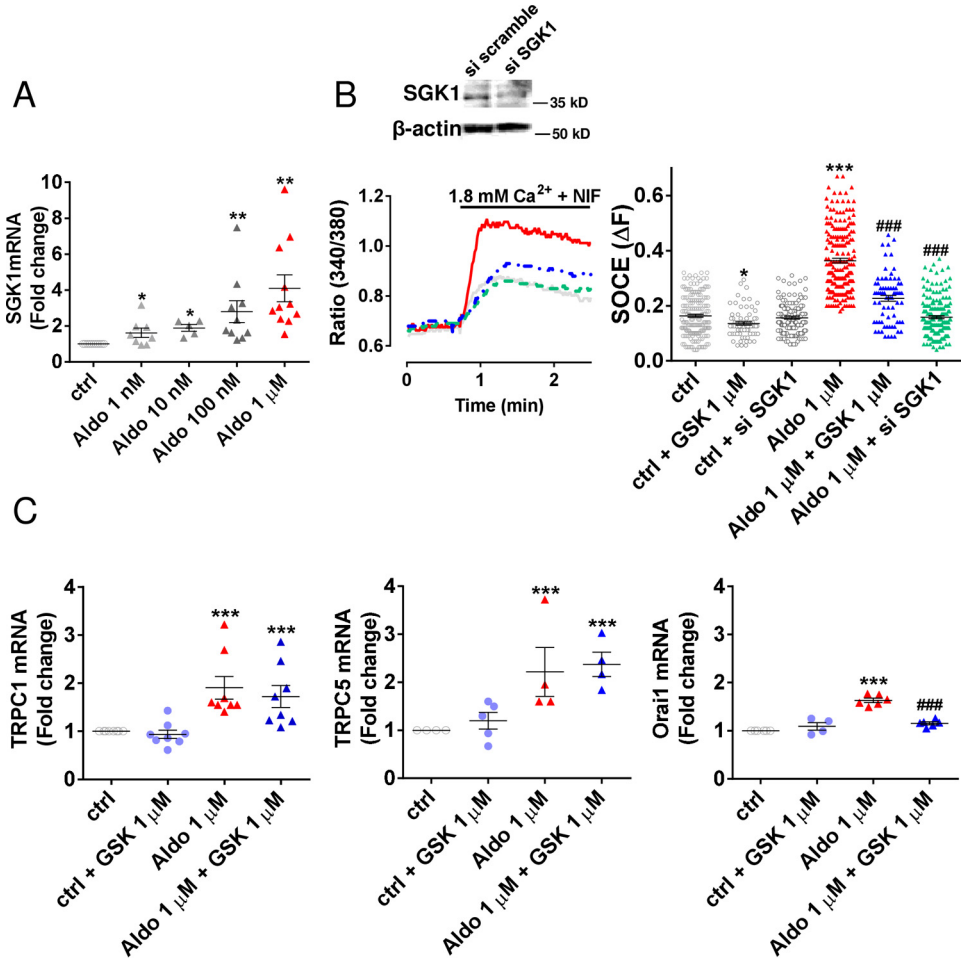

FIGURE 6. **SGK1 inhibition by GSK650394 and silencing by siRNA decrease SOCE and prevent the Orai1-enhanced mRNA expression by aldosterone.** *A*, scatter plots with mean ± S.E. illustrating the relative SGK1 mRNA expression determined by qRT-PCR of NRVMs treated or not with increasing doses of Aldo. *Error bars* represent S.E. *, $p < 0.05$; **, $p < 0.01$ *versus* ctrl; $n = 5–11$ primary cultures. *B*, *left panel*, representative traces of $[Ca^{2+}]_i$ variation measured with Fura-2 fluorescence ratio (340/380) in untreated (ctrl; *light gray* trace) and Aldo-treated NRVMs in the absence (*red* trace) or presence of 1 μM SGK1 inhibitor GSK (*blue* trace) or presence of siRNA against SGK1 (*green* trace). *Right panel*, quantitative assessment of SOCE (Δ*F*). *Error bars* represent S.E. *, $p < 0.05$; ***, $p < 0.001$ *versus* ctrl; ###, $p < 0.001$ *versus* Aldo; $n = 4$ primary cultures; $n = 73–201$ investigated cells. The cells transfected with the non-targeting siRNA (*si scramble*) display the same amount of SOCE compared with untransfected cells (ctrl). The *top panel* illustrates a reduction by 51% of the amount of SGK1 protein after siRNA treatment. $n = 3$ primary cultures. *C*, scatter plots with mean ± S.E. illustrating the relative TRPC1, -C5, and Orai1 mRNA levels determined by qRT-PCR from untreated or aldosterone-treated NRVMs alone or in combination with GSK. *Error bars* represent S.E. ***, $p < 0.001$ *versus* ctrl; ###, $p < 0.001$ *versus* Aldo; $n = 4–8$ primary cultures.

aortic smooth muscle cells and metabolic syndrome chromaffin cells (55, 56)). Pharmacological characterization and quenching of Mn^{2+} by a Fura-2 fluorescence technique provide a fingerprint for SOCE in this effect. We showed that the aldosterone-enhanced cytosolic $[Ca^{2+}]$ elevation following SR depletion is blunted by widely used SOC blockers. The remaining Ca^{2+} entry in control or aldosterone-treated cells that is insensitive to SOC inhibitors suggests the involvement of other transient receptor potential-dependent Ca^{2+} channels. The use of a selective antagonist of MR abolished the enhanced SOCE, suggesting that aldosterone stimulates SOCs via MR activation. Of note, acute aldosterone did not affect SOCE activated by Ca^{2+} store depletion, strongly suggesting a genomic mechanism of aldosterone/MR on SOCs. Molecular screening using qRT-PCR and Western blotting demonstrated that aldosterone treatment for 24 h specifically increased mRNA and protein levels of Orai1, TRPC1, -C4, and -C5 through MR activation.

Using dominant negative pore mutants for TRPC1 and Orai1, TRPC4 mutant, or knockdown of TRPC5 by siRNA strategies, we confirmed that the aldosterone-increased SOCE is mediated by TRPC1, -C4, -C5, and Orai1 proteins. Our results echoed a previous study in metabolic syndrome adrenal chromaffin cells in which aldosterone increases TRPC1 and -C5 expression (55). A comparative analysis of the cardiac transcriptome of aldosterone-treated mice with cardiomyocyte-targeted MR overexpression (MR-Cardio mice) and untreated MR-Cardio mice showed that aldosterone strongly regulates TRPC4 channel(s) (57). More recently, it has been shown that aldosterone significantly elevated the Orai1 transcript level and increased SOCE in UMR106 cells (58). Our study shows for the first time that aldosterone affects SOCE in cardiac myocytes. Importantly, blocking one of these molecular candidates is sufficient to blunt the aldosterone-induced increase of SOCE. This is probably due to the fact that the dn-Orai1 or dn-TRPC was shown to inhibit the function of all Orais or TRPC due to heteromultimerization. Similarly, we found that the co-overexpression of dn-TRPC1 and dn-Orai1, dn-TRPC4 and dn-Orai1 or dn-TRPC1, and dn-TRPC4 mutants did not have an addi-

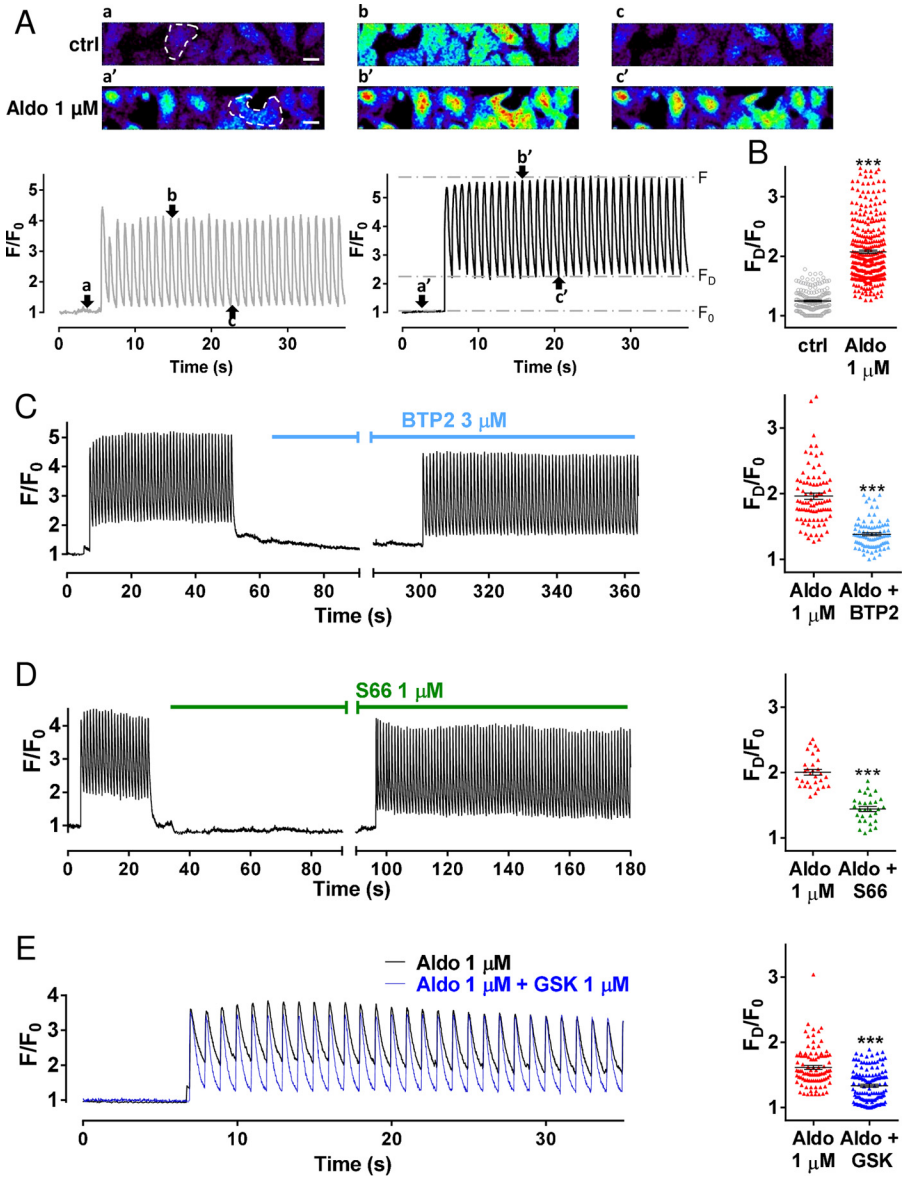

FIGURE 7. **SOC inhibition by BTP2 or Orai1 inhibition by S66 reduces the aldosterone-induced diastolic Ca^{2+} increase.** *A*, representative traces of $[Ca^{2+}]_i$ transients recorded in untreated cells (*gray* trace) or in 1 μM Aldo-treated cells (*black* trace) for 24 h. The *top panels* show confocal images of Fluo-4/AM-loaded untreated NRVMs (ctrl) or 24-h Aldo-treated NRVMs paced at 1 Hz and continuously perfused with normal Tyrode's solution containing 1.8 mM Ca^{2+}. The images correspond to the fluorescence intensity at rest (*a* and *a′*), at the peak (*b* and *b′*), and at the diastolic level (*c* and *c′*). *Scale bars*, 10 μm. *B*, scatter plots with mean ± S.E. illustrating the diastolic Ca^{2+} increase (expressed as peak F_D/F_0) in the ctrl (*open circles*) or Aldo (*red triangles*) condition. *Error bars* represent S.E. ***, $p < 0.001$ *versus* ctrl; $n = 10$ primary cultures; $n = 187–326$ investigated cells. *C*, *left panel*, representative traces of $[Ca^{2+}]_i$ transients recorded in 1 μM Aldo-treated NRVMs before and after exposure to 3 μM BTP2. *Right panel*, scatter plots with mean ± S.E. illustrating the diastolic Ca^{2+} increase during stimulation (expressed as peak F_D/F_0) before (*red triangles*) and after 2–3-min BTP2 (*light blue triangles*) exposure of 24-h Aldo-treated NRVMs. *Error bars* represent S.E. ***, $p < 0.001$ *versus* Aldo; $n = 3$ primary cultures; $n = 86–93$ investigated cells. *D*, *left panel*, representative traces of $[Ca^{2+}]_i$ transients recorded in 1 μM Aldo-treated NRVMs before and after exposure to 1 μM S66. *Right panel*, scatter plots with mean ± S.E. illustrating the diastolic Ca^{2+} increase during stimulation before (*red triangles*) and after 2–3-min S66 (*green triangles*) exposure of 24-h Aldo-treated NRVMs. *Error bars* represent S.E. ***, $p < 0.001$ *versus* Aldo; $n = 3$ primary cultures; $n = 30$ investigated cells. *E*, *left panel*, representative traces of $[Ca^{2+}]_i$ transients recorded in 1 μM Aldo-treated NRVMs with or without 1 μM GSK. *Right panel*, scatter plots with mean ± S.E. illustrating the diastolic Ca^{2+} increase after 24-h treatment with Aldo alone (*red triangles*) or with GSK (*blue triangles*). *Error bars* represent S.E. ***, $p < 0.001$ *versus* Aldo; $n = 4$ primary cultures; $n = 90–121$ investigated cells.

tional effect on SOCE, suggesting that Orai1 might function together with TRPC1 and -C4 and supporting the idea of the heteromultimerization process.

Orai1 has been shown to contribute to the ion permeability of Ca^{2+} release-activated Ca^{2+} channels, which has been reported to be independent of TRPC proteins (59, 60). However, recent studies have proposed that Orai1 proteins might interact with TRPC proteins to form diverse SOCs in a variety of cell types (61). For example, in human atrial myocytes, the SOCs are likely formed by TRPC1, STIM1, and Orai1 (51). It also has been established that activation of STIM1-dependent TRPC1 and -C4 channels, via dynamic interaction, requires functional Orai1. Orai1 interacts with both TRPC4 and -C1 upon endoplasmic reticulum Ca^{2+} store depletion, influencing the Ca^{2+} selectivity of the TRPC1 and -C4 channels (52). A TRPC5/STIM1/Orai1 association in a

stoichiometric manner to enhance SOCE also has been demonstrated (62).

We observed that NRVMs exhibit an endogenous BTP2-sensitive current activated by Ca^{2+} store depletion (I_{SOC}) with a reversal potential near 0 mV and have current properties distinct from Ca^{2+} release-activated Ca^{2+} channels. Indeed, Ca^{2+} release-activated Ca^{2+} channels exhibit a highly Ca^{2+}-selective inward current with a reversal potential near the equilibrium potential for Ca^{2+}. Importantly, I_{SOC} is significantly increased upon aldosterone treatment, confirming our Ca^{2+} imaging data. The characteristics of SOCs in these cells are similar to those described before in other cell types (63, 64) or in adult cardiomyocytes (65, 66). Importantly, non-functional Orai1 mutant significantly reduced aldosterone-enhanced I_{SOC}. This suggests that SOC function requires Orai1 and that TRPC and Orai1 might contribute to the same channel or distinct channels whereby the Orai1 function somehow regulates TRPC channel(s), conferring store-dependent activation of these channels. Co-immunoprecipitation experiments and I_{SOC} properties are consistent with the first possibility because we found that TRPC1, -C4, -C5, Orai1, and STIM1 form a macromolecular complex following Ca^{2+} store depletion, providing strong evidence that there is a close association between TRPC proteins and Orai1. These data show that dynamic assembly of TRPC-STIM1-Orai1 is involved in generating SOCE and concertedly regulates SOCE in NRVMs.

We further investigated the role of the SR-localized Ca^{2+}-sensing protein STIM in activating SOCE. We observed that aldosterone increased protein expression of STIM1 and induced punctum-like formation. This suggests that aldosterone stimulates STIM1 oligomer accumulation into punctum structures at SR-plasmalemmal junctions. Untreated NRVMs expressing the native YFP-WT-STIM1 displayed a high level of SOCE compared with cells transfected with empty plasmid. By contrast, overexpression of native STIM1 in aldosterone-treated cells had no additional effect on SOCE, suggesting a maximal activation of the STIM1-dependent SOCE machinery after aldosterone treatment. Recent studies showed that gating of TRPC channel(s) by STIM1 is mediated by intermolecular electrostatic interaction between repeated Lys-rich domain of STIM1 and the TRPC C terminus (53). Expression of dominant negative STIM1-ΔK significantly decreased SOCE in untreated cells, indicating a requirement of STIM1 and its lysine-rich region to activate SOCE via TRPC channel(s) in cardiomyocytes. The inhibitory effect on SOCE of TRPC4 mutant, with a point mutation in the sequence essential for interaction with STIM1, strengthened the idea of a key role of STIM1 in SOC-dependent signaling. By contrast, in aldosterone-treated cells, we observed a very small effect in enhanced SOCE measured with Ca^{2+} imaging and a non-significant effect on $I_{SOC.}$ These data suggest that this domain is less involved in SOCE in the aldosterone condition. In addition, the fact that dn-Orai1 completely abolished aldosterone-dependent I_{SOC} suggests that up-regulation of Orai1 expression is of major importance in aldosterone-enhanced SOCE.

Orai1/3 as heteropentamers can act as arachidonate-regulated Ca^{2+} channels, which are store-independent Orai channels (67). The fact that Orai3 gene was not affected by aldosterone treatment strengthens the idea of the specific nature of the store-dependent Ca^{2+} entry carried by TRPC1, -C4, -C5, and Orai1 channels. Of note, TRPC3, like receptor-operated channels, did not interact with TRPC1, -C4, -C5, and Orai1 and did not affect the aldosterone-enhanced SOCE, strengthening this idea.

Only high concentrations of aldosterone up-regulate SOCs, indicating an indirect effect of aldosterone/MR signaling in modulating these channels. We then inquired for a possible underlying mechanism. SGK1 was chosen as a plausible candidate due to its previous implication in the regulation of various ion channels, notably STIM1/Orai1 (54). Moreover, SGK1 expression is stimulated by mineralocorticoids (68). Recently, it has been shown that cardiac SGK1 is activated in human and murine HF and that cardiac-specific activation of SGK1 in mice increased mortality, cardiac dysfunction, and ventricular arrhythmias. Conversely, cardiac-specific inhibition of SGK1 protected mice after hemodynamic stress from fibrosis, HF, and induced Na^+ channel alterations (69). In addition, cardiac SGK1 is activated early after pressure overload induced by transverse aortic, and acute activation promotes cardiomyocyte survival (70). Of interest, SGK1 expression (71) and activity (72) are stimulated by increased cytosolic Ca^{2+} activity. Thus, SGK1 could serve as an amplifier of Ca^{2+} entry. Our results demonstrated an up-regulation of SGK1 mRNA expression in NRVMs after aldosterone treatment. In addition, pharmacological inhibition of SGK1 by GSK650394 or silencing by specific SGK1 siRNA strongly reduced the enhanced SOCE. Interestingly, blockade of SGK1 prevented exclusively the increased Orai1 expression induced by aldosterone but not the up-regulation of TRPC1 and -C5. Similarly, recent observations uncovered that SGK1 up-regulates SOCE in both mast cells and platelets through regulation of Orai1 and STIM1 gene expression (54, 58, 73). Thus, these results support the idea of direct targets of MR for TRPC1 and -C5 by the presence of several glucocorticoid response element half-sites in the promoter region (55) and indirect targets of MR for Orai1 via SGK1.

Ca^{2+} is an important regulator in many cardiomyocyte functions such as electrophysiological processes, excitation-contraction coupling, regulation of contractile protein activity, energy metabolism, and transcriptional regulation (74). Consequently, perturbation of its homeostasis leads to life-threatening disease, including hypertrophic cardiac remodeling, arrhythmias, and cell death. We were the first to show that the modulation of voltage-gated Ca^{2+} channels at the plasma membrane (L- and T-type) and of the ryanodine receptor, the Ca^{2+} release channel of the SR, is a central factor in the cardiac aldosterone/MR action and might be involved in triggered afterdepolarization-related fatal ventricular tachyarrhythmia (35–39). SOCE has also emerged as a potential mechanism to alter Ca^{2+} in the cardiomyocyte. It is greatly recognized that Ca^{2+} entry through TRPC1, -C3, -C4, and -C6 channels and STIM1, by changing the fetal gene program governed by calcineurin/NFAT signaling, which is a characteristic of stressed cardiomyocytes, contributes to the pathogenesis of hypertrophy and HF (11, 14, 15, 21–26). Additionally, many studies speculate the potential deleterious effect of SOCs in atrial and ventricular arrhythmias (27, 29, 31, 32). Interestingly, we and

others have demonstrated that TRPC dysfunction could be responsible for the occurrence of ventricular tachycardia (27, 28). In the current study, we showed a diastolic Ca^{2+} increase during field stimulation in NRVMs induced by chronic aldosterone treatment. This increase is totally suppressed when SOCs are inhibited by BTP2 and when Orai1 is specifically blocked by S66 and partially reduced in the presence of the SGK1 inhibitor GSK, suggesting that SOCs contribute to the Ca^{2+} handling at rest through an SGK1-dependent mechanism. Our findings provide direct experimental support for the prediction that SOCs play a key role in regulating cardiac diastolic Ca^{2+} homeostasis.

Taken together, the current study underscores the importance of aldosterone/MR signaling as new regulatory element to exert its influence on TRPC1-, -C4-, -C5-, and Orai1-mediated SOCE in ventricular cardiomyocytes.

Author Contributions—J. S. and J.-P. B. designed the experiments. J. S. and F. B. performed the experiments. J. S., A. M. G., and J.-P. B. wrote the manuscript.

Acknowledgments—We thank Dominique Fortin for excellent technical advices in qRT-PCR and Françoise Boussac for administrative help. We thank the AnimEX for animal care and the Trans-Prot platform IFR141-IPSIT from the University of Paris-Sud.

References

1. Feske, S. (2009) ORAI1 and STIM1 deficiency in human and mice: roles of store-operated Ca^{2+} entry in the immune system and beyond. *Immunol. Rev.* **231,** 189–209
2. Nilius, B., and Szallasi, A. (2014) Transient receptor potential channels as drug targets: from the science of basic research to the art of medicine. *Pharmacol. Rev.* **66,** 676–814
3. Berna-Erro, A., Redondo, P. C., and Rosado, J. A. (2012) Store-operated Ca^{2+} entry. *Adv. Exp. Med. Biol.* **740,** 349–382
4. Huang, G. N., Zeng, W., Kim, J. Y., Yuan, J. P., Han, L., Muallem, S., and Worley, P. F. (2006) STIM1 carboxyl-terminus activates native SOC, I_{crac} and TRPC1 channels. *Nat. Cell Biol.* **8,** 1003–1010
5. Lee, K. P., Choi, S., Hong, J. H., Ahuja, M., Graham, S., Ma, R., So, I., Shin, D. M., Muallem, S., and Yuan, J. P. (2014) Molecular determinants mediating gating of transient receptor potential canonical (TRPC) channels by stromal interaction molecule 1 (STIM1). *J. Biol. Chem.* **289,** 6372–6382
6. Watanabe, H., Murakami, M., Ohba, T., Ono, K., and Ito, H. (2009) The pathological role of transient receptor potential channels in heart disease. *Circ. J.* **73,** 419–427
7. Collins, H. E., Zhu-Mauldin, X., Marchase, R. B., and Chatham, J. C. (2013) STIM1/Orai1-mediated SOCE: current perspectives and potential roles in cardiac function and pathology. *Am. J. Physiol. Heart Circ. Physiol.* **305,** H446–H458
8. Uehara, A., Yasukochi, M., Imanaga, I., Nishi, M., and Takeshima, H. (2002) Store-operated Ca^{2+} entry uncoupled with ryanodine receptor and junctional membrane complex in heart muscle cells. *Cell Calcium* **31,** 89–96
9. Huang, J., van Breemen, C., Kuo, K. H., Hove-Madsen, L., and Tibbits, G. F. (2006) Store-operated Ca^{2+} entry modulates sarcoplasmic reticulum Ca^{2+} loading in neonatal rabbit cardiac ventricular myocytes. *Am. J. Physiol. Cell Physiol.* **290,** C1572–C1582
10. Nakayama, H., Wilkin, B. J., Bodi, I., and Molkentin, J. D. (2006) Calcineurin-dependent cardiomyopathy is activated by TRPC in the adult mouse heart. *FASEB J.* **20,** 1660–1670
11. Onohara, N., Nishida, M., Inoue, R., Kobayashi, H., Sumimoto, H., Sato, Y., Mori, Y., Nagao, T., and Kurose, H. (2006) TRPC3 and TRPC6 are essential for angiotensin II-induced cardiac hypertrophy. *EMBO J.* **25,** 5305–5316
12. Touchberry, C. D., Elmore, C. J., Nguyen, T. M., Andresen, J. J., Zhao, X., Orange, M., Weisleder, N., Brotto, M., Claycomb, W. C., and Wacker, M. J. (2011) Store-operated calcium entry is present in HL-1 cardiomyocytes and contributes to resting calcium. *Biochem. Biophys. Res. Commun.* **416,** 45–50
13. Makarewich, C. A., Zhang, H., Davis, J., Correll, R. N., Trappanese, D. M., Hoffman, N. E., Troupes, C. D., Berretta, R. M., Kubo, H., Madesh, M., Chen, X., Gao, E., Molkentin, J. D., and Houser, S. R. (2014) Transient receptor potential channels contribute to pathological structural and functional remodeling after myocardial infarction. *Circ. Res.* **115,** 567–580
14. Bush, E. W., Hood, D. B., Papst, P. J., Chapo, J. A., Minobe, W., Bristow, M. R., Olson, E. N., and McKinsey, T. A. (2006) Canonical transient receptor potential channels promote cardiomyocyte hypertrophy through activation of calcineurin signaling. *J. Biol. Chem.* **281,** 33487–33496
15. Kuwahara, K., Wang, Y., McAnally, J., Richardson, J. A., Bassel-Duby, R., Hill, J. A., and Olson, E. N. (2006) TRPC6 fulfills a calcineurin signaling circuit during pathologic cardiac remodeling. *J. Clin. Investig.* **116,** 3114–3126
16. Ohba, T., Watanabe, H., Murakami, M., Takahashi, Y., Iino, K., Kuromitsu, S., Mori, Y., Ono, K., Iijima, T., and Ito, H. (2007) Upregulation of TRPC1 in the development of cardiac hypertrophy. *J. Mol. Cell. Cardiol.* **42,** 498–507
17. Zhou, R., Hang, P., Zhu, W., Su, Z., Liang, H., and Du, Z. (2011) Whole genome network analysis of ion channels and connexins in myocardial infarction. *Cell. Physiol. Biochem.* **27,** 299–304
18. Satoh, S., Tanaka, H., Ueda, Y., Oyama, J., Sugano, M., Sumimoto, H., Mori, Y., and Makino, N. (2007) Transient receptor potential (TRP) protein 7 acts as a G protein-activated Ca^{2+} channel mediating angiotensin II-induced myocardial apoptosis. *Mol. Cell. Biochem.* **294,** 205–215
19. Völkers, M., Dolatabadi, N., Gude, N., Most, P., Sussman, M. A., and Hassel, D. (2012) Orai1 deficiency leads to heart failure and skeletal myopathy in zebrafish. *J. Cell Sci.* **125,** 287–294
20. Luo, X., Hojayev, B., Jiang, N., Wang, Z. V., Tandan, S., Rakalin, A., Rothermel, B. A., Gillette, T. G., and Hill, J. A. (2012) STIM1-dependent store-operated Ca^{2+} entry is required for pathological cardiac hypertrophy. *J. Mol. Cell. Cardiol.* **52,** 136–147
21. Wu, X., Eder, P., Chang, B., and Molkentin, J. D. (2010) TRPC channels are necessary mediators of pathologic cardiac hypertrophy. *Proc. Natl. Acad. Sci. U.S.A.* **107,** 7000–7005
22. Hulot, J. S., Fauconnier, J., Ramanujam, D., Chaanine, A., Aubart, F., Sassi, Y., Merkle, S., Cazorla, O., Ouillé, A., Dupuis, M., Hadri, L., Jeong, D., Mühlstedt, S., Schmitt, J., Braun, A., *et al.* (2011) Critical role for stromal interaction molecule 1 in cardiac hypertrophy. *Circulation* **124,** 796–805
23. Voelkers, M., Salz, M., Herzog, N., Frank, D., Dolatabadi, N., Frey, N., Gude, N., Friedrich, O., Koch, W. J., Katus, H. A., Sussman, M. A., and Most, P. (2010) Orai1 and Stim1 regulate normal and hypertrophic growth in cardiomyocytes. *J. Mol. Cell. Cardiol.* **48,** 1329–1334
24. Bénard, L., Oh, J. G., Cacheux, M., Lee, A., Nonnenmacher, M., Matasic, D. S., Kohlbrenner, E., Kho, C., Pavoine, C., Hajjar, R. J., and Hulot, J. S. (2016) Cardiac Stim1 silencing impairs adaptive hypertrophy and promotes heart failure through inactivation of mTORC2/Akt signaling. *Circulation* **133,** 1458–1471
25. Correll, R. N., Goonasekera, S. A., van Berlo, J. H., Burr, A. R., Accornero, F., Zhang, H., Makarewich, C. A., York, A. J., Sargent, M. A., Chen, X., Houser, S. R., and Molkentin, J. D. (2015) STIM1 elevation in the heart results in aberrant Ca^{2+} handling and cardiomyopathy. *J. Mol. Cell. Cardiol.* **87,** 38–47
26. Camacho Londoño, J. E., Tian, Q., Hammer, K., Schröder, L., Camacho Londoño, J., Reil, J. C., He, T., Oberhofer, M., Mannebach, S., Mathar, I., Philipp, S. E., Tabellion, W., Schweda, F., Dietrich, A., Kaestner, L., *et al.* (2015) A background Ca^{2+} entry pathway mediated by TRPC1/TRPC4 is critical for development of pathological cardiac remodelling. *Eur. Heart J.* **36,** 2257–2266
27. Hirose, M., Takeishi, Y., Niizeki, T., Nakada, T., Shimojo, H., Kashihara, T., Horiuchi-Hirose, M., Kubota, I., Mende, U., and Yamada, M. (2011) Diacylglycerol kinase zeta inhibits ventricular tachyarrhythmias in a mouse model of heart failure. *Circ. J.* **75,** 2333–2342

28. Sabourin, J., Robin, E., and Raddatz, E. (2011) A key role of TRPC channels in the regulation of electromechanical activity of the developing heart. *Cardiovasc. Res.* **92,** 226–236
29. Sabourin, J., Antigny, F., Robin, E., Frieden, M., and Raddatz, E. (2012) Activation of transient receptor potential canonical 3 (TRPC3)-mediated Ca^{2+} entry by A1 adenosine receptor in cardiomyocytes disturbs atrioventricular conduction. *J. Biol. Chem.* **287,** 26688–26701
30. Wang, P., Umeda, P. K., Sharifov, O. F., Halloran, B. A., Tabengwa, E., Grenett, H. E., Urthaler, F., and Wolkowicz, P. E. (2012) Evidence that 2-aminoethoxydiphenyl borate provokes fibrillation in perfused rat hearts via voltage-independent calcium channels. *Eur. J. Pharmacol.* **681,** 60–67
31. Doleschal, B., Primessnig, U., Wölkart, G., Wolf, S., Schernthaner, M., Lichtenegger, M., Glasnov, T. N., Kappe, C. O., Mayer, B., Antoons, G., Heinzel, F., Poteser, M., and Groschner, K. (2015) TRPC3 contributes to regulation of cardiac contractility and arrhythmogenesis by dynamic interaction with NCX1. *Cardiovasc. Res.* **106,** 163–173
32. Wolkowicz, P. E., Huang, J., Umeda, P. K., Sharifov, O. F., Tabengwa, E., Halloran, B. A., Urthaler, F., and Grenett, H. E. (2011) Pharmacological evidence for Orai channel activation as a source of cardiac abnormal automaticity. *Eur. J. Pharmacol.* **668,** 208–216
33. Messaoudi, S., Azibani, F., Delcayre, C., and Jaisser, F. (2012) Aldosterone, mineralocorticoid receptor, and heart failure. *Mol. Cell. Endocrinol.* **350,** 266–272
34. Bénitah, J. P., and Vassort, G. (1999) Aldosterone upregulates Ca^{2+} current in adult rat cardiomyocytes. *Circ. Res.* **85,** 1139–1145
35. Bénitah, J. P., Perrier, E., Gómez, A. M., and Vassort, G. (2001) Effects of aldosterone on transient outward K^+ current density in rat ventricular myocytes. *J. Physiol.* **537,** 151–160
36. Perrier, E., Kerfant, B. G., Lalevee, N., Bideaux, P., Rossier, M. F., Richard, S., Gómez, A. M., and Benitah, J. P. (2004) Mineralocorticoid receptor antagonism prevents the electrical remodeling that precedes cellular hypertrophy after myocardial infarction. *Circulation* **110,** 776–783
37. Perrier, R., Richard, S., Sainte-Marie, Y., Rossier, B. C., Jaisser, F., Hummler, E., and Bénitah, J. P. (2005) A direct relationship between plasma aldosterone and cardiac L-type Ca^{2+} current in mice. *J. Physiol.* **569,** 153–162
38. Ouvrard-Pascaud, A., Sainte-Marie, Y., Bénitah, J. P., Perrier, R., Soukaseum, C., Nguyen Dinh Cat, A., Royer, A., Le Quang, K., Charpentier, F., Demolombe, S., Mechta-Grigoriou, F., Beggah, A. T., Maison-Blanche, P., Oblin, M. E., Delcayre, C., *et al.* (2005) Conditional mineralocorticoid receptor expression in the heart leads to life-threatening arrhythmias. *Circulation* **111,** 3025–3033
39. Gómez, A. M., Rueda, A., Sainte-Marie, Y., Pereira, L., Zissimopoulos, S., Zhu, X., Schaub, R., Perrier, E., Perrier, R., Latouche, C., Richard, S., Picot, M. C., Jaisser, F., Lai, F. A., Valdivia, H. H., *et al.* (2009) Mineralocorticoid modulation of cardiac ryanodine receptor activity is associated with downregulation of FK506-binding proteins. *Circulation* **119,** 2179–2187
40. Takeda, Y., Yoneda, T., Demura, M., Usukura, M., and Mabuchi, H. (2002) Calcineurin inhibition attenuates mineralocorticoid-induced cardiac hypertrophy. *Circulation* **105,** 677–679
41. Ferron, L., Ruchon, Y., Renaud, J. F., and Capuano, V. (2011) T-type Ca^{2+} signalling regulates aldosterone-induced CREB activation and cell death through PP2A activation in neonatal cardiomyocytes. *Cardiovasc. Res.* **90,** 105–112
42. He, B. J., Joiner, M. L., Singh, M. V., Luczak, E. D., Swaminathan, P. D., Koval, O. M., Kutschke, W., Allamargot, C., Yang, J., Guan, X., Zimmerman, K., Grumbach, I. M., Weiss, R. M., Spitz, D. R., Sigmund, C. D., *et al.*. (2011) Oxidation of CaMKII determines the cardiotoxic effects of aldosterone. *Nat. Med.* **17,** 1610–1618
43. Kim, M. S., Zeng, W., Yuan, J. P., Shin, D. M., Worley, P. F., and Muallem, S. (2009) Native store-operated Ca^{2+} influx requires the channel function of Orai1 and TRPC1. *J. Biol. Chem.* **284,** 9733–9741
44. Poteser, M., Graziani, A., Eder, P., Yates, A., Mächler, H., Romanin, C., and Groschner, K. (2008) Identification of a rare subset of adipose tissue-resident progenitor cells, which express CD133 and TRPC3 as a VEGF-regulated Ca^{2+} entry channel. *FEBS Lett.* **582,** 2696–2702
45. Liou, J., Fivaz, M., Inoue, T., and Meyer, T. (2007) Live-cell imaging reveals sequential oligomerization and local plasma membrane targeting of stromal interaction molecule 1 after Ca^{2+} store depletion. *Proc. Natl. Acad. Sci. U.S.A.* **104,** 9301–9306
46. Prakriya, M., Feske, S., Gwack, Y., Srikanth, S., Rao, A., and Hogan, P. G. (2006) Orai1 is an essential pore subunit of the CRAC channel. *Nature* **443,** 230–233
47. Sundivakkam, P. C., Freichel, M., Singh, V., Yuan, J. P., Vogel, S. M., Flockerzi, V., Malik, A. B., and Tiruppathi, C. (2012) The Ca^{2+} sensor stromal interaction molecule 1 (STIM1) is necessary and sufficient for the store-operated Ca^{2+} entry function of transient receptor potential canonical (TRPC) 1 and 4 channels in endothelial cells. *Mol. Pharmacol.* **81,** 510–526
48. Li, J., McKeown, L., Ojelabi, O., Stacey, M., Foster, R., O'Regan, D., Porter, K. E., and Beech, D. J. (2011) Nanomolar potency and selectivity of a Ca^{2+} release-activated Ca^{2+} channel inhibitor against store-operated Ca^{2+} entry and migration of vascular smooth muscle cells. *Br. J. Pharmacol.* **164,** 382–393
49. Greka, A., Navarro, B., Oancea, E., Duggan, A., and Clapham, D. E. (2003) TRPC5 is a regulator of hippocampal neurite length and growth cone morphology. *Nat. Neurosci.* **6,** 837–845
50. Ambudkar, I. S., Ong, H. L., Liu, X., Bandyopadhyay, B. C., and Cheng, K. T. (2007) TRPC1: the link between functionally distinct store-operated calcium channels. *Cell Calcium* **42,** 213–223
51. Zhang, Y. H., Wu, H. J., Che, H., Sun, H. Y., Cheng, L. C., Li, X., Au, W. K., Tse, H. F., and Li, G. R. (2013) Functional transient receptor potential canonical type 1 channels in human atrial myocytes. *Pflugers Archiv.* **465,** 1439–1449
52. Cioffi, D. L., Wu, S., Chen, H., Alexeyev, M., St Croix, C. M., Pitt, B. R., Uhlig, S., and Stevens, T. (2012) Orai1 determines calcium selectivity of an endogenous TRPC heterotetramer channel. *Circ. Res.* **110,** 1435–1444
53. Zeng, W., Yuan, J. P., Kim, M. S., Choi, Y. J., Huang, G. N., Worley, P. F., and Muallem, S. (2008) STIM1 gates TRPC channels, but not Orai1, by electrostatic interaction. *Mol. Cell* **32,** 439–448
54. Lang, F., Münzer, P., Gawaz, M., and Borst, O. (2013) Regulation of STIM1/Orai1-dependent Ca^{2+} signalling in platelets. *Thromb. Haemost.* **110,** 925–930
55. Hu, G., Oboukhova, E. A., Kumar, S., Sturek, M., and Obukhov, A. G. (2009) Canonical transient receptor potential channels expression is elevated in a porcine model of metabolic syndrome. *Mol. Endocrinol.* **23,** 689–699
56. Bae, Y. M., Kim, A., Lee, Y. J., Lim, W., Noh, Y. H., Kim, E. J., Kim, J., Kim, T. K., Park, S. W., Kim, B., Cho, S. I., Kim, D. K., and Ho, W. K. (2007) Enhancement of receptor-operated cation current and TRPC6 expression in arterial smooth muscle cells of deoxycorticosterone acetate-salt hypertensive rats. *J. Hypertens.* **25,** 809–817
57. Messaoudi, S., Gravez, B., Tarjus, A., Pelloux, V., Ouvrard-Pascaud, A., Delcayre, C., Samuel, J., Launay, J. M., Sierra-Ramos, C., Alvarez de la Rosa, D., Clément, K., Farman, N., and Jaisser, F. (2013) Aldosterone-specific activation of cardiomyocyte mineralocorticoid receptor *in vivo*. *Hypertension* **61,** 361–367
58. Zhang, B., Umbach, A. T., Chen, H., Yan, J., Fakhri, H., Fajol, A., Salker, M. S., Spichtig, D., Daryadel, A., Wagner, C. A., Föller, M., and Lang, F. (2016) Up-regulation of FGF23 release by aldosterone. *Biochem. Biophys. Res. Commun.* **470,** 384–390
59. DeHaven, W. I., Jones, B. F., Petranka, J. G., Smyth, J. T., Tomita, T., Bird, G. S., and Putney, J. W., Jr. (2009) TRPC channels function independently of STIM1 and Orai1. *J. Physiol.* **587,** 2275–2298
60. Ong, H. L., Cheng, K. T., Liu, X., Bandyopadhyay, B. C., Paria, B. C., Soboloff, J., Pani, B., Gwack, Y., Srikanth, S., Singh, B. B., Gill, D. L., and Ambudkar, I. S. (2007) Dynamic assembly of TRPC1-STIM1-Orai1 ternary complex is involved in store-operated calcium influx. Evidence for similarities in store-operated and calcium release-activated calcium channel components. *J. Biol. Chem.* **282,** 9105–9116
61. Cheng, K. T., Ong, H. L., Liu, X., and Ambudkar, I. S. (2013) Contribution and regulation of TRPC channels in store-operated Ca^{2+} entry. *Curr. Top. Membr.* **71,** 149–179
62. Ma, H. T., Peng, Z., Hiragun, T., Iwaki, S., Gilfillan, A. M., and Beaven, M. A. (2008) Canonical transient receptor potential 5 channel in conjunction with Orai1 and STIM1 allows Sr^{2+} entry, optimal influx of Ca^{2+}, and

degranulation in a rat mast cell line. *J. Immunol.* **180,** 2233–2239
63. Yuan, J. P., Zeng, W., Huang, G. N., Worley, P. F., and Muallem, S. (2007) STIM1 heteromultimerizes TRPC channels to determine their function as store-operated channels. *Nat. Cell Biol.* **9,** 636–645
64. Cheng, K. T., Liu, X., Ong, H. L., and Ambudkar, I. S. (2008) Functional requirement for Orai1 in store-operated TRPC1-STIM1 channels. *J. Biol. Chem.* **283,** 12935–12940
65. Kojima, A., Kitagawa, H., Omatsu-Kanbe, M., Matsuura, H., and Nosaka, S. (2012) Presence of store-operated Ca^{2+} entry in C57BL/6J mouse ventricular myocytes and its suppression by sevoflurane. *Br. J. Anaesth.* **109,** 352–360
66. Domínguez-Rodríguez, A., Ruiz-Hurtado, G., Sabourin, J., Gómez, A. M., Alvarez, J. L., and Benitah, J. P. (2015) Proarrhythmic effect of sustained EPAC activation on TRPC3/4 in rat ventricular cardiomyocytes. *J. Mol. Cell. Cardiol.* **87,** 74–78
67. Thompson, J. L., Mignen, O., and Shuttleworth, T. J. (2013) The ARC channel—an endogenous store-independent Orai channel. *Curr. Top. Membr.* **71,** 125–148
68. Shigaev, A., Asher, C., Latter, H., Garty, H., and Reuveny, E. (2000) Regulation of sgk by aldosterone and its effects on the epithelial Na^+ channel. *Am. J. Physiol. Renal Physiol.* **278,** F613–F619
69. Das, S., Aiba, T., Rosenberg, M., Hessler, K., Xiao, C., Quintero, P. A., Ottaviano, F. G., Knight, A. C., Graham, E. L., Boström, P., Morissette, M. R., del Monte, F., Begley, M. J., Cantley, L. C., Ellinor, P. T., *et al.* (2012) Pathological role of serum- and glucocorticoid-regulated kinase 1 in adverse ventricular remodeling. *Circulation* **126,** 2208–2219
70. Aoyama, T., Matsui, T., Novikov, M., Park, J., Hemmings, B., and Rosenzweig, A. (2005) Serum and glucocorticoid-responsive kinase-1 regulates cardiomyocyte survival and hypertrophic response. *Circulation* **111,** 1652–1659
71. Taruno, A., Niisato, N., and Marunaka, Y. (2008) Intracellular calcium plays a role as the second messenger of hypotonic stress in gene regulation of SGK1 and ENaC in renal epithelial A6 cells. *Am. J. Physiol. Renal Physiol.* **294,** F177–F186
72. Imai, S., Okayama, N., Shimizu, M., and Itoh, M. (2003) Increased intracellular calcium activates serum and glucocorticoid-inducible kinase 1 (SGK1) through a calmodulin-calcium calmodulin dependent kinase kinase pathway in Chinese hamster ovary cells. *Life Sci.* **72,** 2199–2209
73. Borst, O., Schmidt, E. M., Münzer, P., Schönberger, T., Towhid, S. T., Elvers, M., Leibrock, C., Schmid, E., Eylenstein, A., Kuhl, D., May, A. E., Gawaz, M., and Lang, F. (2012) The serum- and glucocorticoid-inducible kinase 1 (SGK1) influences platelet calcium signaling and function by regulation of Orai1 expression in megakaryocytes. *Blood* **119,** 251–261
74. Gómez, A. M., Ruiz-Hurtado, G., Benitah, J. P., and Domínguez-Rodríguez, A. (2013) Ca^{2+} fluxes involvement in gene expression during cardiac hypertrophy. *Curr. Vasc. Pharmacol.* **11,** 497–506
75. Grynkiewicz, G., Poenie, M., and Tsien, R. Y. (1985) A new generation of Ca^{2+} indicators with greatly improved fluorescence properties. *J. Biol. Chem.* **260,** 3440–3450